MEASUREMENTS OF LAMINAR BURNING SPEEDS OF MIXTURES OF PROPANE AND CARBON DIOXIDE AT ELEVATED TEMPERATURES AND PRESSURES

A Thesis Presented

By

Khalid Aljohani

to

The Department of Mechanical and Industrial Engineering

In partial fulfillment of the requirements for the degree of

Master of Science

In the field of

Mechanical Engineering

Northeastern University

Boston, Massachusetts

August 2018

ABSTRACT

In recent years, as the expanding of alternative refrigerant working fluids are being intimately considered in terms of its less environmental consequences, a mixture with excellent thermodynamic properties is emerging, propane (C_3H_8) with the addition of carbon dioxide (CO_2) concentrations. The main reason that led the propane kept restricted as alternative refrigerant working fluids is its high flammability characteristic. This mixture can be utilized as a substitute working fluid in refrigeration systems since it's relied solely on naturally occurring compound (hydrocarbon) as well as has an excellent ozone depletion potential (ODP), and more importantly with a very good global warming potential (GWP), compared to other chlorofluorocarbon CFHs and Hydrofluorocarbons HFCs. It has been clearly evaluated that the combination of propane (C_3H_8) with additional of carbon dioxide (CO_2) as diluent own no challenge to the environment. Moreover, the Environmental Protection Agency (EPA) has approved the use of propane in systems specially intended to control its flammability characteristic. In this thesis, a mixture of propane (C_3H_8) with diluent of carbon dioxide (CO_2) has been introduced as a new substitute blend in order to reduce the propane flammability as well as the high pressure that gained by the carbon dioxide (CO_2). These suggestions were made based on the blend's thermodynamics properties, low toxicity, low global warming potentials (GWP), and negligible ozone-depletion potentials (ODP). The laminar burning speed and flame structures of spherically expanding flames of propane (C_3H_8) with air have been studied over a wide range of additional carbon dioxide (CO_2) concentrations, at various range of equivalence ratios, elevated temperatures, and pressures. The laminar burning speeds of propane-air with added carbon dioxide mixtures have been measured in the pressure ranging from 0.5 to 4 atmospheres, and temperatures ranging from 400 to 600 K for different equivalence ratios. The range of equivalence ratios implemented in this work was between 0.8 to 1.2. The experimental study has been conducted using a constant-volume cylindrical combustion chamber which is fitted well in a Z-type Schlieren shadowgraph system. The cylindrical chamber was heated by utilizing band heaters around the two-ends of the chamber. By a thermodynamic analysis, the laminar burning speed was calculated using the primary input of pressure-time records that was obtained in the duration of combustion process.

ACKNOWLEDGMENT

I would like to thank my research advisors Professor Hameed Metghalchi and Professor Yiannis Levendis for their guidance, effort, and endless support both in the coursework and the research. I also would like to further send many thanks to the laboratory team; Bassam S. Aljohani, and Ziyu Wang.

Dedicated to my parents Saad and Affaf for offering me the opportunity to attend Northeastern and also for always being supporting and motivating.

Dedicated to my wife Saja for her patient and motivational words when I need them throughout this journey, I could not have done it without you.

Table of Contents

List of Figures

1. Introduction

This chapter is an overview of the importance of the determination of laminar burning speeds and the different experimental approaches used to measure the burning speeds will be demonstrated.

1.1. Background

The study of determining the burning speed rates of homogeneous gaseous fuels and diluent mixtures is critically utmost importance for the improvement of chemical kinetic as well as fluid dynamic model that involves fuel oxidation both of which would contribute to the advancement of a wide range of many practical applications such as engines, power plants, chemical processors, and air conditioning systems. In particular, overall efficiency improvement and emission reduction can be easily achieved by determining the unburned gases of the combustible mixture which is one part of studying the laminar burning rate at elevated temperatures and pressures. As alternative blends are continually becoming environmentally friendly into many fields such as AC system there is a need to determine the flammability characteristic as well as the laminar burning speed rates of theses mixtures for safety purposes as well as in calibrating and validating many of such mechanisms.

Laminar burning speed is a basic thermo-physical property and can be defined as the direct determination of the rate of energy released in the combustion duration process of a combustible mixture which is a function of pressure, temperature, and the mixture composition.

1.2. Experimental approaches of determining Burning Speed

For determining burning speed, the two widely used methods can be summarized according to the flame characteristic; stationary flame technique and propagating flame technique. Although there are other various techniques have been utilized for the calculation of burning speeds by different researchers such as Linnett [1], Andrews [2], and Rallis [3] and have obtained careful reviews of the previous measurement methods. In this section, a detailed view of the two above-mentioned methods will be clearly demonstrated.

1.2.1 Stationary Flame Methods

Examples of stationary flame methods are; flat flame burners, stagnation flames, and nozzle methods. The method used in flat flame burners is allowing a flow of combustible mixtures passes into the stationary flame and when the unburned gas rate arrives, this rate is assumed to be equal to the laminar burning speed of the gas. In this method, there is a lack of collected burning speed measurements that may results in inaccurate data. The burner energy loss is another concern for flat burner method since it reduces the exactness data of flat flame technique. Botha and Spalding have worked on the developing of the flat burner methods using a variation technique for preventing the burner energy losses [4]. To illustrate, the researchers have controlled the flame in a way that would allow the experimentalists to record the temperature rise of the cover at various rates of fuel stream as well as the determination of peak adiabatic flame temperature was predicted by the known ratio of volumetric flow rate to the flame disc area.

The second technique is called nozzle stationary flame where Bunsen burner type flames used. Bunsen burner type with needle valve produces a single open gas flame in which the velocity distribution is parabolic at exist. This shows that the inclination of the flame surfaces is changing along the flame, while it should be curved that counterparts with the assumption that the flame is a conical in shape. And as result, the accuracy of Bunsen burner types lies within the geometrical difficulties of the flame. For accurate results, Linteris's experiment has encountered issues with stretch effects and Bunsen type design and suggested a future work regarding a new design that would minimize the stretch effects [5].

The stagnation flame method or the counter flow method is utilized to measure the flame burning speed of a combustible mixture and was developed by Wu and Law [6], and Egolfopoulos [7]. The way this technique work is that the interaction point of contact has an ignition source and two similar flows of premixed combustible mixtures are propagating towards the ignition source/that point. Additionally, Kim and Matalon have developed adequate solutions particularly on the standoff point as well as the extinction curve analysis which explains the thermal expansion variations [8]. The inaccuracy of the counter flow method lies within the numerical data that is obtained for determining the velocity profiles assuming zero gradient point.

1.2.2 Propagating Flames Methods

Propagating flames techniques mainly are divided into two classifications; cylindrical flame tube method and propagating spherical flame method. The cylindrical flame tube is a horizontal in shape and opened at one end where the mixture is ignited. Mallard and Le Chatelier developed the cylindrical flame tube method and theorized that the flame is propagating by a heat conduction source outwardly to the combustion zone, the closed end, where the flame is assumed to be self-sustaining and the progressing flame rate must be raised to the ignition temperature of the mixture [9]. Moreover, the researchers have assumed that the flame burning speed along the tube is constant and that where the inaccuracy of the burning speed data lies. Not only this but also the heat conduction energy losses by the flame to the tube wall is decreasing the flame burning speed rate.

The other method in which will be used in this study is the propagating spherical flame. This method is individualized into two parts; propagating flame with pressure-constant and propagating flame with volume-constant. Metghalchi and Eisazadeh-Far has developed the spherical propagating flame with uniform pressure using an accurate system called shadowgraph system [10]. Furthermore, they assumed that the first phase of combustion event the chemical composition of the mixture is in equilibrium and the pressure is distributed uniformly among the species which have constant pressure. Because of the rapid compression during combustion, the researchers theorized that the burned and unburned gasses are compressed isentropically. Another primary assumption is that the flame is perfectly spherical in shape, smooth, and unwrinkled. The reason the shadowgraph

system utilized is because of its capabilities capturing the combustion development during the whole event as well as the ability of measuring the flame radius as a function of time. The inaccuracy of propagating flame with pressure-constant method lies within the energy losses due to radiation, electrode conduction energy losses, and ignition box voltage variations. Constant volume and constant pressure propagating flame techniques are considered to be the utmost experimental accurate method that utilizes the pressure rise records during combustion event. The following type of spherically propagating flames is constant volume method. In this method, a thermodynamics model is employed for the determination of the laminar burning speed data in which the mass fraction rate of burned gasses obtained to calculate the burning speed. Lewis and Von Elbe were the first developers of this technique [11] followed by a similar method that was developed by Metghalchi and Keck [12-13]. Metghalchi and Keck have applied this method to a constant-volume combustion vessel that uses the pressure rise records obtained through the duration of combustion.

In this thesis, the constant volume propagating flame combustion vessel method is used for the determination of laminar flame burning velocity. The main advantages of manipulating this method are as follows; numerous data points along the isentrop are easily collected in a single experiment without involving an extrapolation work. Additionally, the effect of an Ac electric field in spherical flames behavior using the constant volume combustion vessel method have been investigated by Shinichi and Cha and concluded that the ignition source has insufficient influence on changing the laminar burning rates [14 -15]. Moreover, the DC ignition event under spherically expanding flames was studied by Meng [20] and reported that electric fields might develop the flame propagation and reduces the duration of overall combustion. This would enhance the assumption validity that burned and unburned gasses are compressed isentropically. For detailed description on the thermodynamics analysis with constant volume vessel, in chapter 3.

2. Experimental Facilities and Methods

In this chapter, the overview of the equipment laboratory and detailed procedures are described thoroughly. Additionally, the setup utilized in the combustion components, shadowgraph system, gas delivery system, heating system, and ignition system are clearly demonstrated.

2.1 Laboratory Facilities

Cylindrical Combustion Vessel:

The cylindrical combustion vessel dimensions are; 133.35mm in length, and has an internal diameter of 135 mm, and is made of 316 stainless steel. The two ends of the cylindrical vessel have two Pyrex windows that are 35 mm thick each and serve for the investigation of the flame structure and combustion duration. Moreover, the Pyrex windows are sealed with O-rings and capable to stand for high temperature as well as pressure ranges, to maximum of 500K and 50 atm. In addition, the windows provide the needed viewing angle in such a way that allowing the light source passes throughout the vessel for the purpose of recording the combustion development, this is called a Z-type Shadowgraph system and is discussed in the following section. In regard to the heating system, two band heaters are directly connected to each end of the chamber and a detailed description is given in the next section. The required pressure of the cylindrical vessel can be managed by a Kistler 603B1 piezoelectric pressure transducer that utilizes the 5010B charge amplifier to convert a 4-20 mA signal obtained from the pressure transducer into a 10mV/psi signal. To acquire the wall vessel pressure, the use of digital conversion box is needed to record the pressure variations at the wall in the course of combustion process. Pressure date and flame structures are obtained by the use of LabVIEW software and a digital camera. The cylindrical combustion vessel can be seen in figure 1-2, and 3.

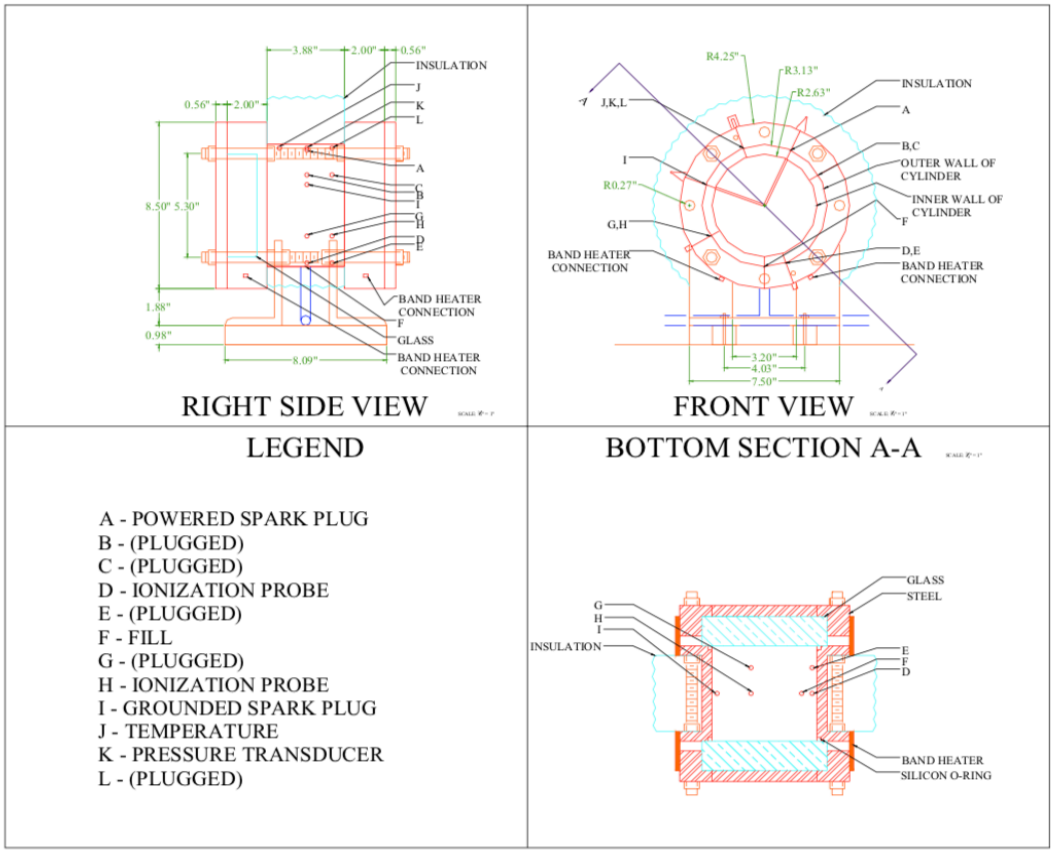

Figure 1: Illustration of the dimensions of the cylindrical combustion chamber

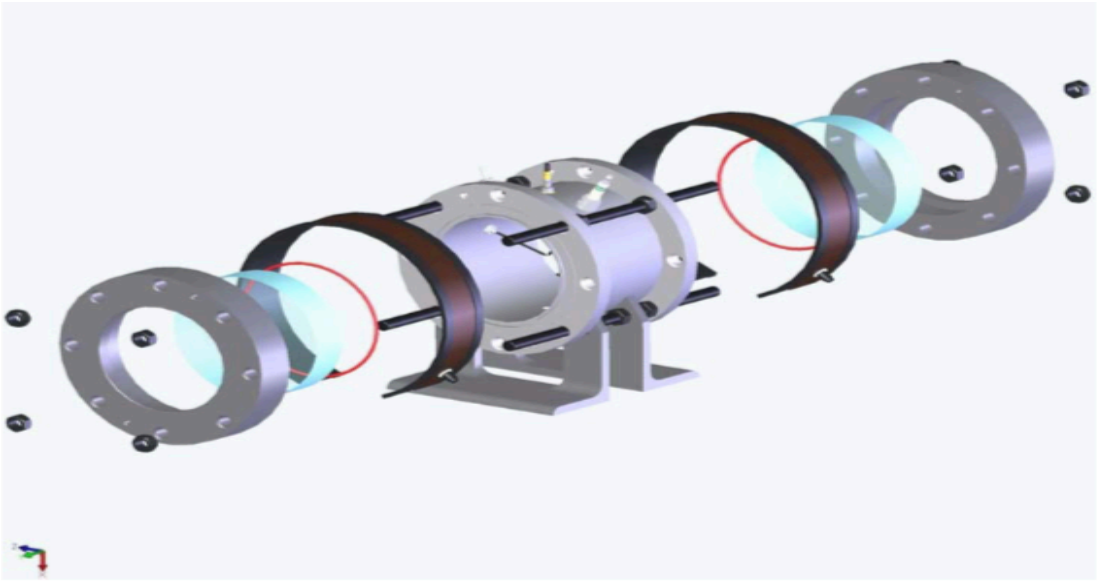

Figure 2: A modelling of the combustion chamber showing each component

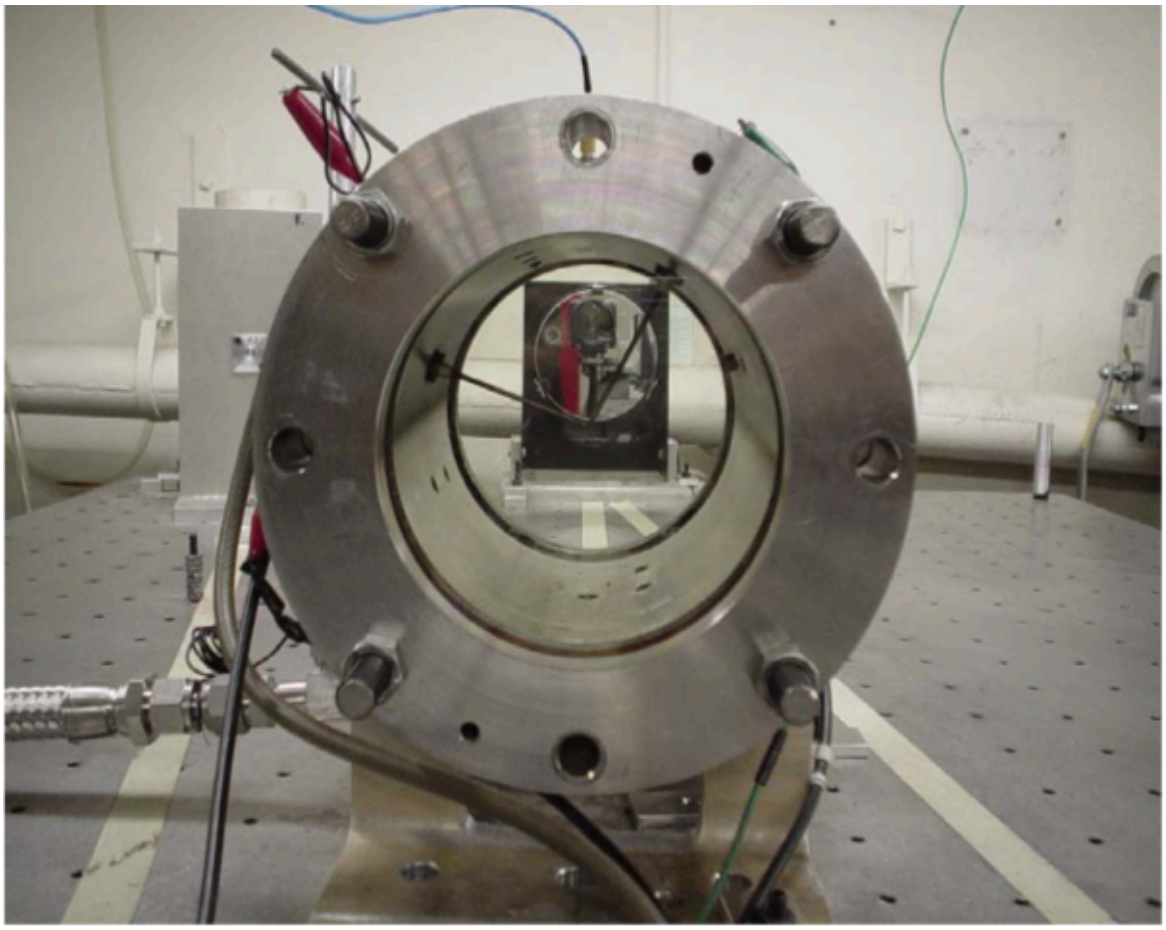

Figure 3: A front-view of the cylindrical chamber showing the inner surface where the flame propagates downward.

2.2 Z-type Schlieren Design

For the testing chamber, the Z-type Shadowgraph assembly is responsible of filming the flame propagation as well as flame structure during combustion as shown in figure 4 and 5. Two spherical mirrors are separately fixed on two opposite ends of the vessel and have identical diameters of 152.4 mm with focal length of 1524 mm. The 10-Watt Halogen lamp are centered precisely behind the chamber in order to maintain the light passes through 0.3mm diameter hollow providing an intense illumination for the system. A high-speed CMOS camera (HG-LE, Redlake Inc.) has been placed with a 15-degree angle on the opposite side of mirror 2. The CMOS camera is capable of capturing 40,000 frames per second with high accuracy of the gas mixture density variations within the chamber in the duration of combustion. The inception of the spark until the flame touches the chamber wall is accurately recorded by the CMOS camera and the variation of pressure data is then analyzed accordingly. The purpose of the CMOS camera is the verification and visually inspection of flame geometry, instability, propagation and structure. This configuration works as follow; the light source hits mirror 1, mirror 1 reflects the light and passes it throughout the chamber where mirror 2 is located, the reflection of mirror 2 is then being recorded by CMOS camera, this scenario takes place in milliseconds.

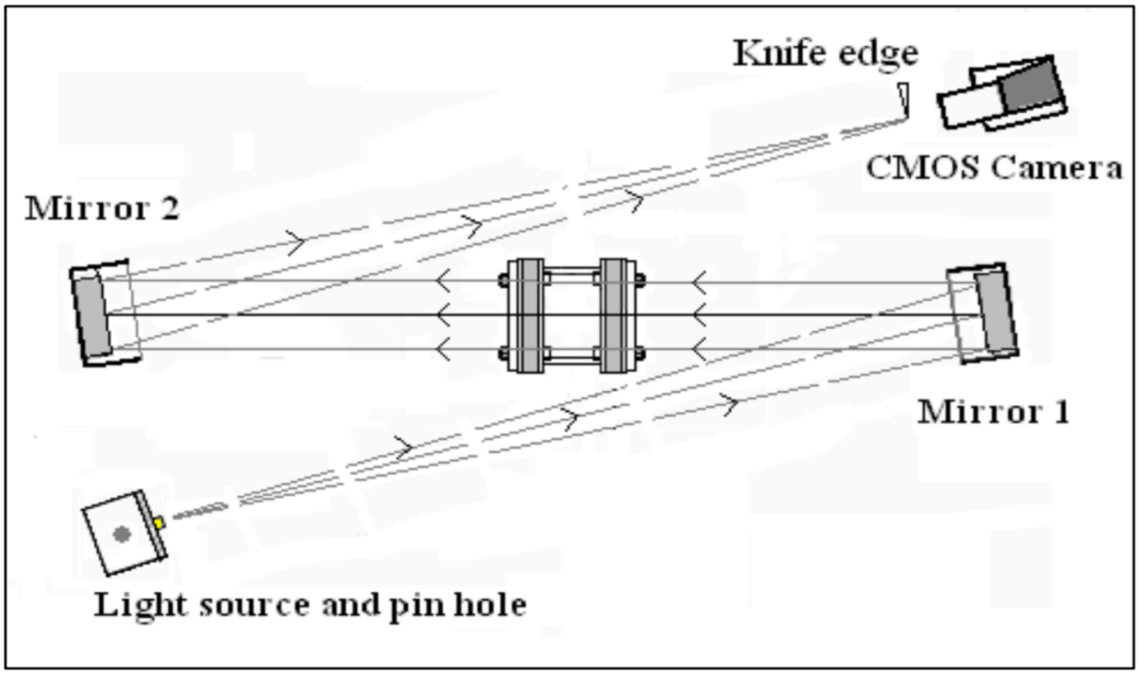

Figure 4: A demonstration of the Z-type Schlieren set up and shadowgraph system implanted in the experiments

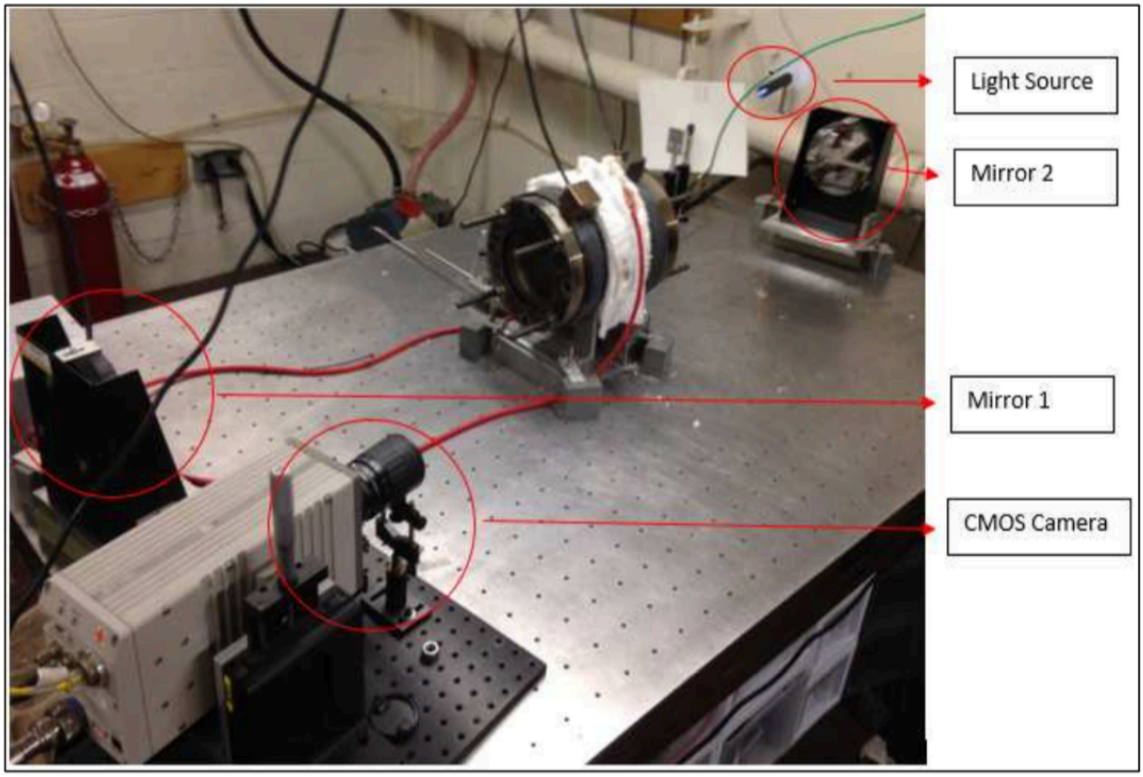

Figure 5: This shows the Z-type Shadowgraph assembly with each numbered component.

2.3 Gas Manifold System

The gas manifold system is connected to the testing chamber by pipes that are being utilized for the distribution of each desired component such as fuels, diluents, and oxidants at their partial pressures. In addition, the gas manifold pipes and the cylindrical chamber are vacuumed by a vacuum pump after each experiment, typically 20 minutes, to maintain accurate results. Another significant purpose of the vacuum pump is to evacuate the lines upon the completion of filling each component to its partial pressure to the chamber. During the gas delivery process, four pressure gauges are considered as illustrated in Figure 7. The top left gauge is called a thermocouple gauge and is designed for calculating the chamber pressure which should be vacuumed to approximately 100 millitorr. The others are piezoelectric pressure transducers with variety of operation ranges; 0-15psi, 0-30psi, and 0-50 psi respectively. The pressure gauge operation ranges depend on the conducted test, the desired pressure of an experiment determines the pressure gauge limit and accordingly the pressure gauge range is selected. The filling measurement process of partial pressures is controlled by the series of valves and transducers. The configuration of the gas manifold system, pressure gauges, valves and transducers are shown in Figure 6.

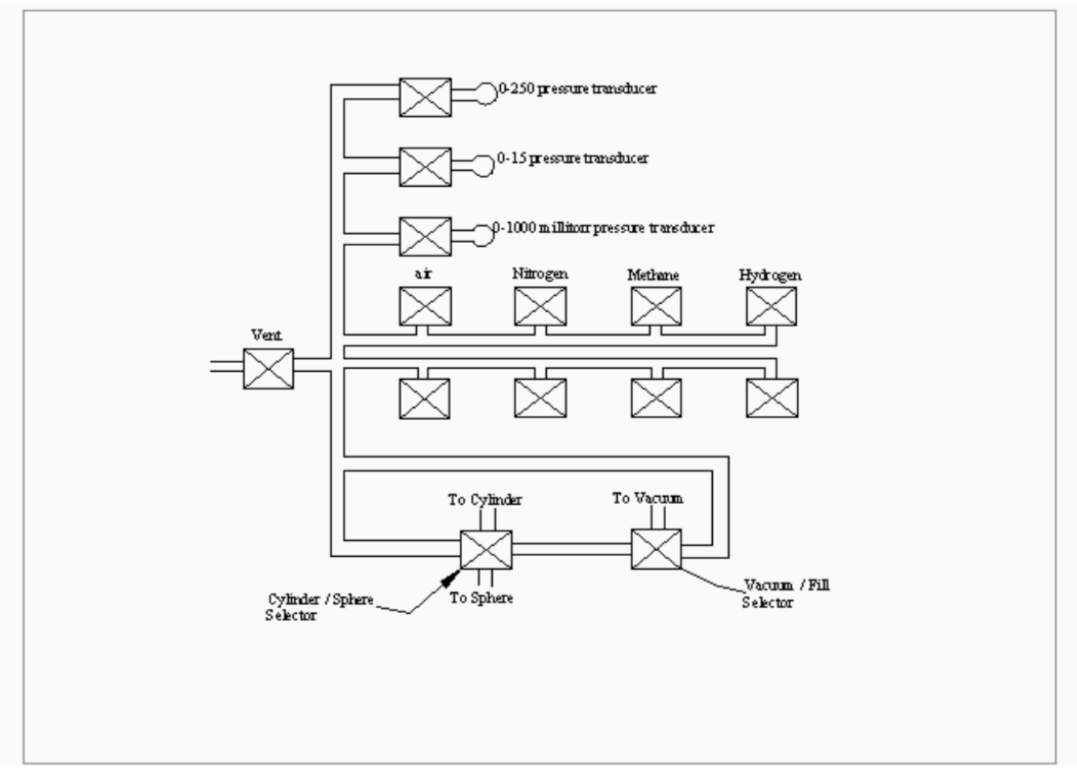

Figure 6: A configuration of the gas manifold system, valves, and transducers

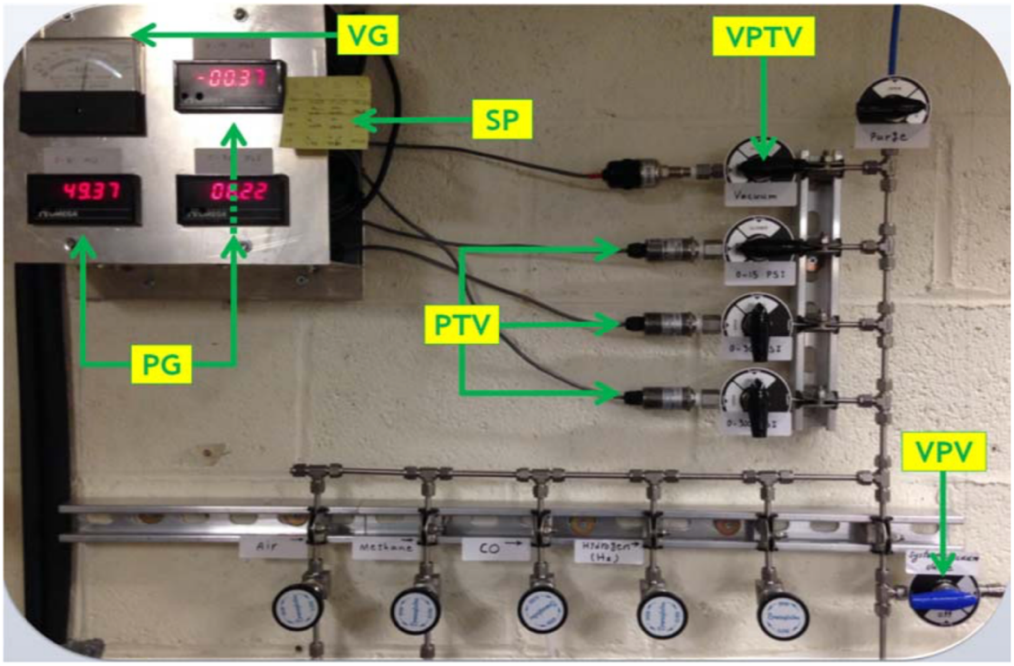

Figure 7: The gas manifold system with the pressure gauges reading used for filling process.

2.4 Heating System

For room-temperature experiments, this section might be neglect and the experimentalists can start the experimenting when pressure gauge reaches 100 millitorr. For conducting elevated temperature experiments, the maximum heating capacity of the cylindrical vessel that can be achieved is approximately 500K. The chamber is heated by using 1.5kW band heaters bolted to the flanges and attached on either end of chamber as demonstrated in Figure 8. The outside wall of the cylinder is covered by two layers of ½" ceramic insulation and the two windows left uncovered for inspection investigations as shown in Figure 8. Additionally, the desired temperature can be sat up easily by AT-BBA-200 PID on-off controllers that show when the vessel exposed heating cycles. The next section presents heating cycles overview and temperature variations.

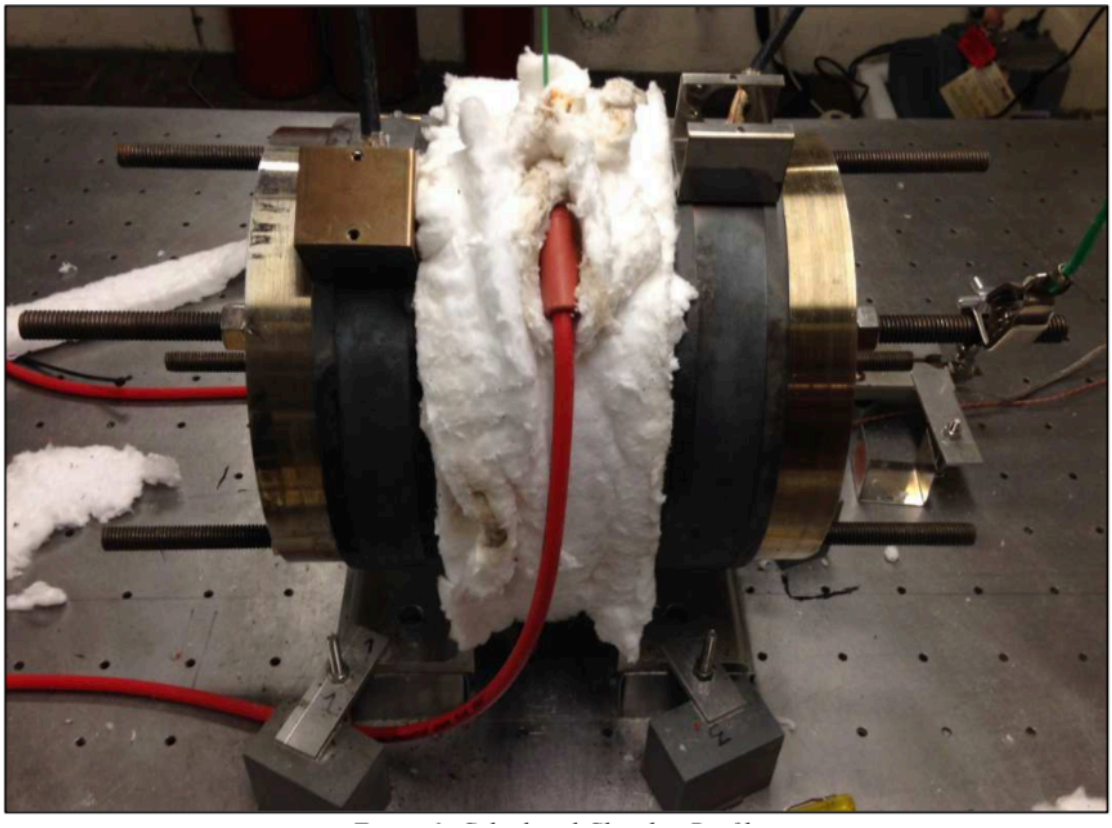

Figure 8: The black-colored band heaters attached to each end of the combustion vessel

2.5 Temperature variations

It has been highly recommended that the elevated temperature of a gas mixture has to be defined accurately for the determination of laminar burning speed as considered to be a strong factor changing the pressure and burning speed data continuously. During experiments, a considerable issue has been noticed which is the temperature of the chamber surface and temperature of combustible mixture were slightly varied, and the higher elevated temperature results in higher variations. The temperature data were collected by two thermocouple K types attached to two different axial locations on the chamber surface. Moreover, number of different experiments performed to find out a correlation between the gas and chamber temperatures as well as the correlation values were tabulated. Furthermore, when filling the vessel, the combustion rapid expansion causes increasing in the gas mixture temperature and this would affect the burning speed. To avoid this, it is noticed that if the combustible mixture was left for adequate time allowing the gases reaches to its equilibrium state as well as allowing the gases to distribute evenly, this would allow the combustible mixture temperature to be reduced to its previous temperature.

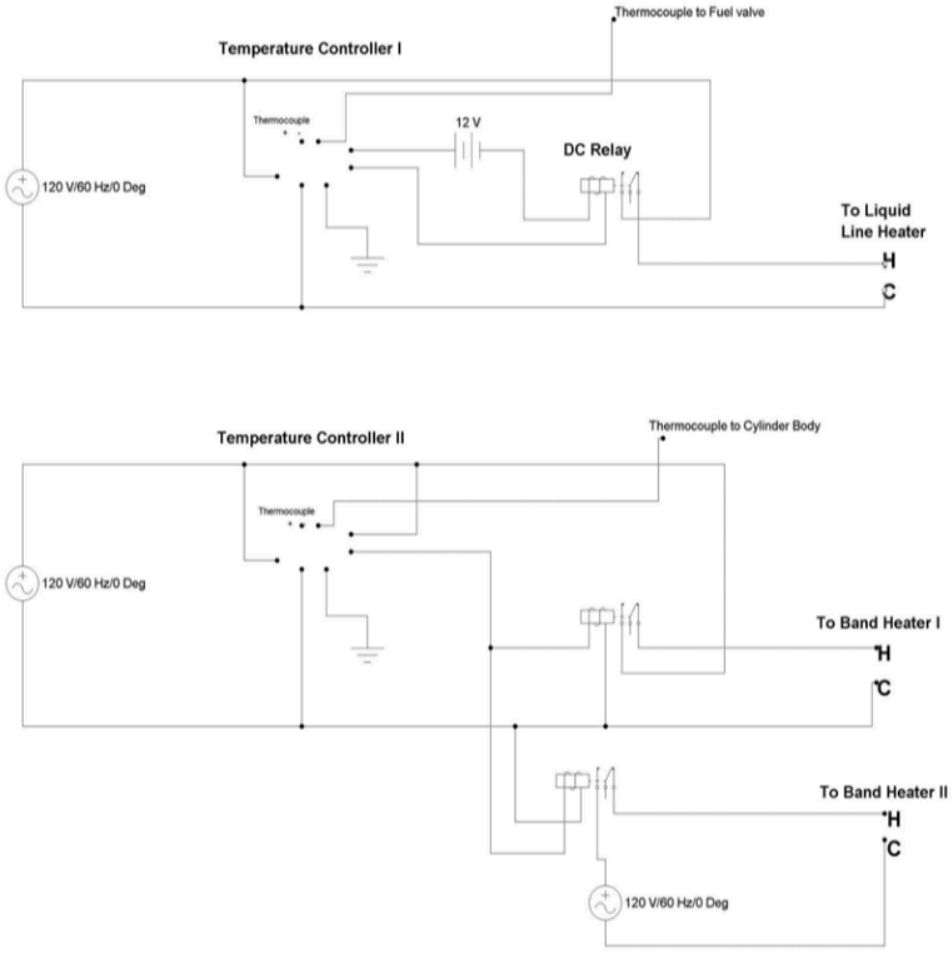

Figure 9: Illustration of the electrical circuits connected to the two-end band heaters by the temperature controllers.

2.6 Ignition System

The ignition source is utilized in activation the reaction process of the combustible mixture in the cylindrical chamber. The cylindrical chamber ignition system comprised of a power output source, a transformer circuit, and two extended length automotive spark plugs. An AC isolated transformer power source is used to generate the power supply source ensuring that the chamber will neither experience premature ignition nor voltage data errors that may result in damaging the system. Upon completion of this part, the capacitor is then will be charged by a converted DC source that was initiated from the AC power source. Subsequently, the use of LabVIEW to generate a trigger needs to be sat up in order to allow the ignition takes place in the chamber. Then, the spark will be initiated at the tips of each electrode leading to ignition in the combustible mixture. In regard to the design of the extended length automotive spark plugs, stainless steel wire with diameter of 0.4mm has been welded to each sparkplug centers, see Figure 3. To illustrate, the extended length spark plugs are inserted into the chamber, from the top allowing the flame to be spherically propagating, and the tips of the spark plugs are distanced from each other by nearly 1mm at the center of the chamber as seen in Figure 10.

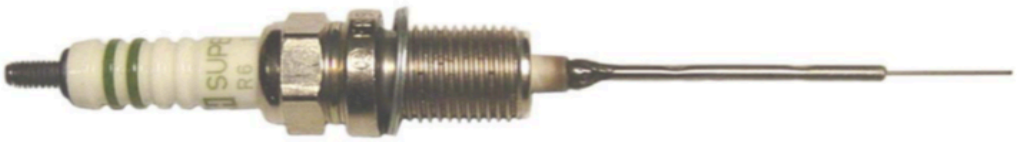

Figure 10: An extended length automotive spark plug, responsible for initiating a spark to combustion occurs

2.7 Experimental Procedure

First of all, the testing chamber and the connected pipes have to be sufficiently evacuated before injecting the gas mixture to the testing chamber. Technically speaking, until the pressure gauge reads approximately 100 millitorr, and this process can be achieved by the pump. Additionally, a spread sheet Excel file has been developed on the basis of various variables such as the pressure transducers zero offset, the fuel to air ratio ϕ, and the added diluents concentrations α, for determining the required partial pressure of each component; a detailed calculation can be seen in the following section. Once the vessel and the pipes have been evacuated, the filling process utilizing the gas manifold can be begun on the basis of the determined partial pressure of each specific component. In this study, the gases filled include Propane C_3H_8, Carbon dioxide CO_2, and air. The filling process order is also based on the predefined initial conditions that were obtained by the spread sheet, and thus for accurate data, it is recommended to begin with the lowest partial pressure values first, followed by the higher partial pressure ones for each component.

This part presents the filling process procedures and requirements for conducting combustible mixture measurements. To demonstrate the filling order, the chamber valve has to be opened allowing the gas mixture to go into the chamber while maintaining the vacuum valve closed, then start to fill the first component until its required partial pressure achieved. At this time, the chamber has to be closed immediately and the lines have to be vacuumed to 100 millitorr again. Then, the next component is filled up to its partial pressure raised beyond the first partial pressure component, in this moment the chamber valve has to be reopened allowing the gas to entre and then proceed filling until its partial pressure reached. In this way, the gasses will neither involve in backflow affect nor premixing of gasses within lines. The last component usually is the air since it has the largest partial pressure, and it is filled as the second step discussed previously. Upon the completion of the filling process the chamber valve is closed and the combustible mixture has to be left for adequate time allowing the gasses to distribute evenly and reach to its equilibrium state. Furthermore, the testing desired temperature has been increased during the filling process as explained previously and the given time will serve the temperature to be brought back to its correlated value.

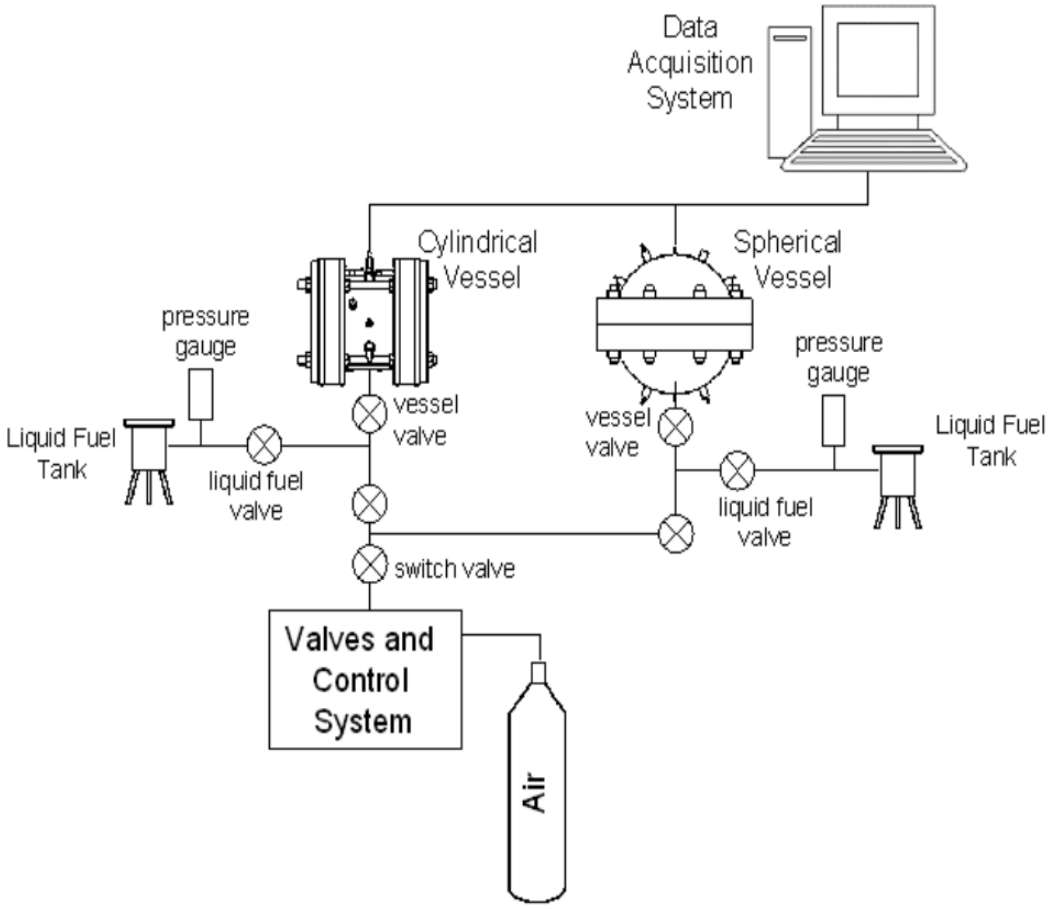

Figure 11: A full demonstration of the facility used during combustion experiments

2.8 Experimental Error Sources

In this study, each case of an experiment has to be repeated several times in order to acquire the utmost right data by matching several pressure-rise records for one condition tested. This section demonstrates the experimental errors resulted within the experimentations duration. There are various number of sources have been observed during experimentations, and data analysis upon completion of the testing. These experimental errors can be described as follow; first the Excel file sheet was developed based on various variables such as zero-offset partial pressure and used for the calculation to determine the expected partial pressure transducer values, it was revealed that this method carries about 1% error. Furthermore, personal accuracy obtained through using the selected transducer for filling the tested vessel can be reached between +/- 1% errors. The total acquisition system that is responsible for producing the pressure signal may contain nearly 2% errors. Additionally, the noise generated during testing was considered in the calculation of the pressure rise variations curve; this procedure carried the largest source of data analysis errors ranging from 2% to 5%. As result, the combination of the errors during experimentations and data analysis can be varied between 4% and 9% as maximum, which is still stood to be acceptable accurate data. Lastly, the careful use of testing can be easily seen resulting in accurate data and it is highly recommended.

2.9 Calculation of Global Reaction Procedure

Alkane hydrocarbons global reaction schemes at different Air- Fuel mixtures (Lean, stoichiometric, and rich mixtures) are shown as respectively:

$$C_a\,H_b + \frac{\left(a + \frac{b}{4}\right)}{\phi}\,(\,0.21\,O_2 + 0.79\,N_2) \rightarrow Products\ of\ Combustion \tag{1}$$

$$When\ \phi < 0, prodcuts\ are: CO_2, H_2O, H_2, and\ N_2$$

$$When\ \phi = 1, prodcuts\ are: CO_2, H_2O, and\ N_2$$

$$When\ \phi \geq 1{,}2\ , prodcuts\ are: CO_2, H_2O, H_2, O_2, and\ N_2$$

In this study, the calculation of premixed combustion of Propane, carbon dioxides, and air mixtures are determined as:

$$\phi[(1-\alpha)\ C_3\ H_8 +\ \alpha\ CO2] + 5(1-\ \alpha)(\ O_2 + 3.76N_2) \rightarrow Products \qquad (2)$$

Where α indicates the diluent concentration. The mole fraction of each component is obtained from:

$$x_i = \frac{n_i}{n_{tot}} \qquad (3)$$

$$x_{C_3H_8} = \frac{n_{C_3H_8}}{n_{tot}} = \frac{\phi(1-\alpha)}{\phi + (1-\ \alpha)(23.80)}$$

$$x_{CO_2} = \frac{n_{CO_2}}{n_{tot}} = \frac{\phi\ \alpha}{\phi + (1-\ \alpha)(23.80)}$$

$$x_{Air} = \frac{n_{Air}}{n_{tot}} = \frac{(1-\ \alpha)(23.80)}{\phi + (1-\ \alpha)(23.80)}$$

$$n_{tot} = n_{fuel} + n_{Air} \ = \ \phi + (1-\ \alpha)(23.80)$$

Determination of partial pressure of each reactant can be found by using the molar fraction method as follows:

$$p_i = \ p_{tot}\ x_i \qquad (4)$$

$$p_{C_3H_8} = \ p_{tot}\ x_{C_3H_8} \ = \ p_{tot}\ \frac{\phi(1-\alpha)}{\phi + (1-\ \alpha)(23.80)}$$

$$p_{CO_2} = \ p_{tot}\ x_{CO_2} = \ p_{tot}\ \frac{\phi\ \alpha}{\phi + (1-\ \alpha)(23.80)}$$

$$p_{Air} = \ p_{tot}\ x_{Air} = \ p_{tot}\ \frac{(1-\ \alpha)(23.80)}{\phi + (1-\ \alpha)(23.80)}$$

For verification and accuracy, the summation of partial pressures and the molar fractions of each species in the reactants should be equal to the total pressure and the total molar fractions of the reaction, hence:

$$x_{tot} = \frac{n_{C_3H_8} + n_{CO_2} + n_{Air}}{n_{tot}} = 1 \tag{5}$$

$$p_{tot} = p_{desired} = p_{C_3H_8} + p_{CO_2} + p_{Air}$$

3. Thermodynamics of Combustion

Metghalchi and Keck (1980-1982) have developed a thermodynamic model that is employed to determine laminar burning speed measurements of premixed flames from the pressure-time records [12-13]. Of this method, one of the advantages of measuring the laminar burning speed using the pressure rise techniques is that a wide range of pressures and temperatures data can collected by a single experiment. This model was modified based on the previous works [17] and a few corrections were added. The investigation is valid for constant pressure data measurements in cylindrical vessel. The assumptions involved in the analysis are as follows:

- The gases distributed in the closed-combustion chamber are grouped into burned and unburned regions separated by preheat and a reaction zones as shown in Fig. 12.
- The unburned and burned gases are assumed to be compressed isentropically as well as behaving as ideal gasses in both regions.
- The pressure is locally uniform and constant through the chamber at any specified time throughout the combustion duration.
- The reaction flame front is thin, smooth, spherical and unwrinkled.
- For a radius larger than 2-3 cm, the flame thickness is negligible. This can be reachable when the pressure-time records start to rise.
- Buoyancy effects are neglected.

Burned gases assumption: The Burned gasses region is consisting of various n number of shells started from the center of the chamber. The n shells can be used to represent the combustion time duration as well as the total values of pressure points. Each shell has a uniform temperature and varies from one shell to another with the assumption that the gases are at chemical equilibrium. Unburned gases assumption: Initially, at rest and have a uniform temperature and a fixed composition.

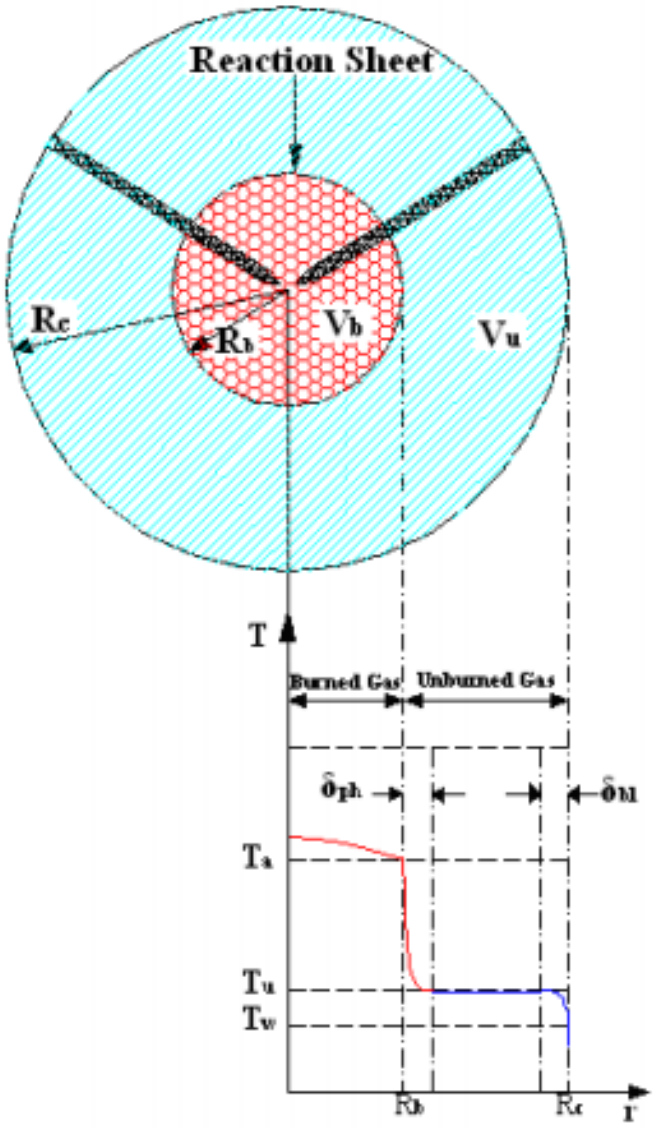

Figure 12: An illustration of the burned and unburned regions associated with each temperature profile.

3.1 Burning Speed Model Analysis:

Based on the assumption mentioned above, the volume and energy equations are derived as:

The ideal gas equation of state:

$$pv = RT \tag{6}$$

$$P = \rho RT \tag{7}$$

Where, p is the total pressure in the chamber, v is the specific volume, R is the specific gas constant ($\bar{R}/_{M}$) and T is the temperature in Kelvin.

As the gas mixtures within the combustion bomb include burned and unburned gases, the conservation equation of the total mass, using Eq. (1), becomes:

$$m_t = m_b + m_u = \frac{p_i}{RT_i} (V_c - V_e) \tag{8}$$

Where m_t is the total mass of gas in the combustion chamber, m_b is the mass of burned gases, m_u is the mass of unburned gasses, V_c and V_e are the volume of the combustion chamber and the volume of electrode, respectively, and i is referring to the initial conditions. Now, consider the total volume of the gas in the combustion chamber is:

$$V_t = V_c - V_e = V_b + V_u = \int_0^{m_b} v_b \, dm + \int_{m_b}^{m_t} v_u \, dm \tag{9}$$

3.2 Burned Gas; Volume Analysis

The volume of burned gas composed of two components. The first component when the volume is compressed isentropically. The other when the gas is involved in the displacement volume. Hence, the volume of the burned gas V_b is:

$$V_b = \int_0^{m_b} v_{b\infty}\, dm - V_{eb} \tag{10}$$

Where, $v_{b\infty}$ is the isentropically compressed specific volume of the burned gases and V_{eb} is the displacement volume of the electrode boundary layer (eb). This volume can be defined as:

$$V_{eb} = \int \left(v_{b\infty} - v_{b,eb} \right)\, dm \tag{11}$$

It can be assumed that the total volume of the combustion V_c is expanded by V_{eb} since the transferring of energy that is by electrodes is decreasing the displacement thickness temperature than the remaining gases temperature in the burned gas region. Therefore, the gas density has to be higher. Then, Eq. (5) can be rewritten using the ideal gas relation as:

$$V_b = \int_0^{m_b} v_b \; dm = \int_0^{m_b} v_{b\infty}\, dm - \frac{R}{P} \int \left(T_{eb,\infty} - T_{eb} \right) \; dm \tag{12}$$

The mass coordinate is illustrated as $dm = A\, d\eta$, thus:

$$V_b = \int_0^{m_b} v_b \; dm$$
$$= \int_0^{m_b} v_{b\infty} \; dm - \frac{R\,T_{eb,\infty}}{P} A \int \left(1 - \frac{T_{eb}}{T_{eb,\infty}}\right) \; d\eta \tag{13}$$

Introducing the general definition of displacement thickness (δ**):**

$$\rho_\infty \delta = \int_0^\infty \left(1 - \frac{T}{T_\infty}\right) \tag{14}$$

Substitute equation (9) into equation (8):

$$V_b = \int_0^{m_b} v_b \; dm = \int_0^{m_b} v_{b\infty} \; dm - \frac{R\,T_{eb,\infty}}{P} A_{eb} \; (\rho_{\infty,\mathrm{eb}} \delta_{eb}) \tag{15}$$

Ultimately, the second term V_{eb} can be expressed as:

$$V_{eb} = A_{eb}\, \delta_{eb} \tag{16}$$

Then, the volume of the burned gases becomes:

$$V_b = \int_0^{m_b} v_b \; dm = \int_0^{m_b} v_{b\infty} \; dm - A_{eb}\, \delta_{eb} \tag{17}$$

3.3 Unburned Gas; Volume Analysis

In order to determine the volume of unburned gasses, the volume of preheat and the thermal boundary zones need to be considered. Figure 12 shows clearly the two-included zones within the volume of the unburned gases.

The volume of unburned gas equation demonstrated as:

$$V_u = \int_{m_b}^{m_t} v_{u\infty}\, dm - V_p - V_w \tag{18}$$

$$V_u = (1 - x_b)\, m v_{u,\infty} - V_p - V_w$$

The first term $v_{u\infty}$ represents the specific volume of the gas when the gas compressed isentropically, V_p is the volume when the gas is preheated, and the last term V_w states when the gas is in the thermal boundary layer which conducting energy loss to the combustion wall. In a similar way as the volume of the electrode of the burned gas V_{eb}. Both V_p and V_w can be showed as:

The volume of the preheat zone:

$$V_w = \int (v_{u,\infty} - v_{u,w})\, dm \tag{19}$$

Where $v_{u,\infty}$ represents the specific volume of unburned gases when compressed isentropically, $v_{u,w}$ is the specific volume of unburned gases at the wall.

The volume of the thermal boundary layer zone:

$$V_p = \int (v_{u,\infty} - v_{u,p})\, dm \tag{20}$$

Where $v_{u,w}$ is the specific volume of unburned gases at the preheat zone.

It can be assumed that the total volume of the combustion V_c is expanded by V_w since the transferring of energy is decreasing the displacement thickness temperature than the other gases temperature in the unburned gas region. Therefore, the gas density has to be higher. On the other hand, assuming that the total volume of the combustion V_c is compressed by

the preheat volume V_p since the transferring of energy is increasing the displacement thickness temperature than the rest gases temperature in the unburned gas region. Therefore, the gas density has to be lower.

Apply Ideal gas law Eq. (2) to Eq. (14), and (15), obtaining:

$$V_w = \frac{R}{P} \int (T_{w,\infty} - T_w) \; dm \tag{21}$$

$$V_p = \frac{R}{P} \int (T_{p,\infty} - T_p) \; dm \tag{22}$$

Using the defined mass coordinate and the defined general displacement thickness Eq. (9), the volume of the thermal boundary layer as well as the volume of the preheat zone could be written as:

$$\mathrm{V_w} = \frac{\mathrm{R\,T_{w,\infty}}}{\mathrm{P}} \mathrm{A_w} \int (1 - \frac{\mathrm{T_w}}{\mathrm{T_{w,\infty}}}) \; \mathrm{d\eta} \tag{23}$$

$$V_p = \frac{R\,T_{p,\infty}}{P} A_p \int (1 - \frac{T_p}{T_{p,\infty}}) \; d\eta \tag{24}$$

The two volumes would become:

$$V_w = \frac{R\,T_{w,\infty}}{P} A_w \left(\rho_{\infty,\mathrm{w}} \delta_w\right) = A_w\,\delta_w \tag{25}$$

$$V_p = \frac{R\,T_{p,\infty}}{P} A_p \left(\rho_{\infty,\mathrm{p}} \delta_p\right) = A_p\,\delta_p \tag{26}$$

Additionally, the areas of each region can be revealed as:

$$\begin{aligned} A_{eb} &= 2\,\pi\, r_e r_b \\ A_w &= 4\,\pi\, r^2 \\ A_p &= 4\,\pi\, r_b^2 \end{aligned} \tag{27}$$

Where r_e is the radius of the electrodes, r_b is the radius of the burned gas, r is the radius of the combustion chamber. A_{eb} is the area of the extended electrode as shown in Figure 12. A_w and $A_p$are the areas of the wall boundary layer and the preheat zone, respectively. δ_w is defined as the displacement thickness of the wall boundary layer, δ_p is the displacement thickness of the preheat zone in front of the reaction layer as shown in Figure 12.

The relation of the displacement thickness of each region can be demonstrated using the simplified expressions derived by Metghalchi and Keck [12-13]:

The displacement thickness of the electrode boundary layer is defined:

$$\delta_{eb} = \frac{2}{3}\left(\frac{T_b}{T_w} - 1\right)\sqrt{\frac{r_b \alpha_b}{\dot{r_b}}} \tag{28}$$

The displacement thickness of the wall boundary layer δ_w was expressed by Keck (Keck 1981) as:

$$\delta_w = \mathcal{Z}^{\frac{-1}{\gamma_u}}\sqrt{\frac{\tau\,\alpha_b}{r_b}}\int_0^{\mathcal{Z}}\left(\mathcal{Z}' - \mathcal{Z}'^{\frac{1}{\gamma_u}}\right)\frac{1}{\sqrt{\int_{\mathcal{Z}'}^{\mathcal{Z}} \mathcal{Z}''\; d\mathcal{Z}''}}\,dy \tag{29}$$

Assuming an approximation using Exponential temperature profile for preheat zone, the displacement thickness of the preheat zone δ_p was evaluated as:

$$\delta_p = -\frac{\alpha_u}{\dot{r_b}}\left(\frac{T_b}{T_u} - 1\right)\ln\frac{T_b}{T_u} \tag{30}$$

Where T_b and T_w are the temperatures of the wall and burned gas, respectively. α_b and α_u are the thermal diffusivity of the burned gas as well as the thermal diffusivity of the unburned gas, respectively. τ is a characteristic burning time, $y = \frac{t}{\tau}$ and $\mathcal{Z} = \frac{p}{p_i}$ are the unitless time and pressure, respectively. It worth mentioning that the displacement thickness of the thermal boundary layers are positive values while the preheat zone has a negative sign.

Ultimately, the volume conservation equation of the burned and unburned gases is expressed as:

$$V_c - V_e + V_{eb} + V_w + V_p = \int_0^{m_b} v_{b,\infty}\ dm + (1 - x_b)\, m\, v_{u,\infty} \tag{31}$$

Substituting equations (11), (20) (21) and (22), the conservation of volume equation becomes:

$$\frac{V_c - V_e}{m} + \frac{2\,\pi\, r_e r_b \delta_{eb} + 4\,\pi\, r^2 \delta_w + 4\,\pi\, r_b^2 \delta_p}{m} = \int_0^{m_b} v_{b,\infty}\ dm + (1 - x_b)\, m\, v_{u,\infty} \tag{32}$$

The conservation of energy equation is:

$$E - Q_e - Q_w - Q_r = E_b + E_u \tag{33}$$

Where E is the unburned gas initial energy, Q_e is the conduction energy loss to the electrodes, Q_w is the conduction energy loss to the wall, and Q_r is the radiation energy loss associated from the burned gases.

3.4 Burned Gas; Energy Analysis

The energy of the burned gas E_b is illustrated as:

$$E_b = \int_0^{m_b} e_b \; dm = \int_0^{m_b} e_{b\infty}\, dm - E_{eb} \tag{34}$$

Where $e_{b,\infty}$ represents the specific energy of burned gases when compressed isentropically, E_{eb} is the energy defect of the electrode boundary layer in the burned gases region, and is expressed using the equation of state Eq. (1) and the defined displacement thickness Eq. (9), as follow:

$$E_{eb} = \int (e_{b,\infty} - e_{b,eb})\; dm \tag{35}$$

$$E_{eb} = c_v \int (T_{b,\infty} - T_{b,eb})\; dm = c_v A_{eb} T_{b,\infty} \int (1 - \frac{T_{eb}}{T_{b,\infty}})\; d\eta \tag{36}$$

$$E_{eb} = c_v A_{eb} T_{b,\infty} \rho_{\infty,eb} \delta_{eb} \tag{37}$$

Now consider the ideal gas equation, $R = c_p - c_v$, where c_p and c_v are the ratio of constant pressure specific heat and the ratio of the constant volume specific heat, respectively, and $\gamma = \frac{c_p}{c_v}$ is the specific gas constant. Then, obtain:

$$E_{eb} = \frac{P\,V_{eb}}{\gamma_b - 1} \tag{38}$$

3.5 Unburned Gas; Energy Analysis

The energy of the unburned gas E_u is demonstrated as:

$$E_u = \int_{m_b}^{m} e_u \; dm = \int_{m}^{m} e_{u\infty}\, dm - E_w - E_p \tag{39}$$

Where $e_{u,\infty}$ represents the specific energy of unburned gases when compressed isentropically, E_w and E_p are the energy defects of the wall boundary layer and the in the preheat zone, respectively, in the unburned gases region. These energy defects can be simplified using the assumption that the gases are compressed isentropically. Also, the equation of state Eq. (1) and the defined displacement thickness Eq. (9) will be used as follow:

$$E_w = \int \left(e_{u,\infty} - e_{u,w} \right) dm \tag{40}$$

$$E_w = c_v \int \left(T_{u,\infty} - T_{u,w} \right) dm = c_v\, A_w T_{u,\infty} \int \left(1 - \frac{T_w}{T_{u,\infty}} \right) \mathrm{d}\eta \tag{41}$$

$$E_w = c_v\, A_w\, T_{u,\infty}\, \rho_{\infty,w} \delta_w \tag{42}$$

Employing the ideal gas relation R, and specific heat constants c_v , c_p, the energy defect of the wall boundary layer E_w , and in a similar way, the energy defect of the preheat zone determined as:

$$E_w = \frac{P\,V_w}{\gamma_u - 1} \tag{43}$$

$$E_p = \frac{P\,V_p}{\gamma_u - 1} \tag{44}$$

Then using Eq. (33), (38) and (39), into Eq. (29) and (34), the conservation of energy equation of the burned and unburned gas becomes:

$$E_b = \int_0^{m_b} e_b \;\; dm \; = \int_0^{m_b} e_{b\infty}\, dm - \frac{P\,V_{eb}}{\gamma_b - 1} \tag{45}$$

$$E_u = \int_{m_b}^{m} e_u \;\; dm \; = \int_{m}^{m} e_{u\infty}\, dm - \frac{P\,V_w}{\gamma_u - 1} - \frac{P\,V_p}{\gamma_u - 1} \tag{46}$$

One approach for determining the conduction energy losses during constant volume combustion and an increasing pressure is to utilize a developed one-dimensional heat conduction equation, that was derived by Keck, for finding the heat transfer between burned and unburned gases, which defined as:

$$\dot{q} = \frac{p}{\tau(\gamma - 1)} \left(\delta + \gamma p \frac{d\delta}{dp}\right) \tag{47}$$

Where τ is the characteristic burning time when pressure rising, $\tau = \frac{p}{\frac{dp}{dt}}$ Using Eq. (42) to determine the heat flux, integrating by part, gives:

$$q'' = \int_0^t \dot{q} \;\; dt \; = \int_0^t \left(\frac{p\delta}{p\,(\gamma - 1)} \frac{dp}{dt} + \frac{\gamma}{\gamma - 1} + \frac{p^2}{p} \frac{dp}{dt} \frac{d\delta}{dp}\right) dt \tag{48}$$

$$q'' = \frac{1}{\gamma - 1}\left(\int_0^t \delta \ \frac{dp}{dt}\ dt + \int_0^t \gamma p \ \frac{d\delta}{dp}\ dt\right) = \frac{\gamma}{(\gamma - 1)}\ p\delta - \int_0^p \delta \ dp \tag{49}$$

Applying the ideal gas relations, Eq. (1) and constant specific heats $R = c_p - c_v$, and the specific gas constant $\gamma = \frac{c_p}{c_v}$, Eq. (44) becomes:

$$Q = q'' A = A\, c_p\, \rho\, T\, \delta - A\int_0^p \delta \ dp \tag{50}$$

Another Approach for Determining Energy Losses:

In terms of the conduction energy losses during constant volume combustion and a rapid elevating pressure, the conduction energy losses are approximately equal to the energy defects in the boundary layer and the preheat zone since the total compression work w_t terms are neglected. However, this case will result in increasing the experimental errors and therefore flame burning speed would be slightly not in an accurately value and thus will not be used in this calculation. However, if this is the case, Eq. (33), (38) and (39) can be approximated to:

$$E_{eb} = \frac{P\, V_{eb}}{\gamma_b - 1} \approx Q_e \tag{51}$$

$$E_w = \frac{P\, V_w}{\gamma_u - 1} \approx Q_w \tag{52}$$

In the burned gas region, the radiation energy loss was calculated using:

$$Q_r = \int_0^t \dot{Q}_r \; dt = 4\,\alpha_p \sigma\, V_b\, (T_b^4 - T_w^4) \tag{53}$$

Where $\dot{Q}_r$ is the rate of radiation, α_p is the Planck mean absorption coefficient and σ is the Stefan Boltzmann constant.

$$\alpha_p = \frac{1}{p_t} \sum (\alpha_i\, p_i) \tag{54}$$

The conservation of energy equation Eq. (28) becomes:

$$\frac{E}{m} - \frac{Q_w + E_w}{m} - \frac{Q_r}{m} = \int_0^{m_b} e_b \; dm \; + \; (1 - x_b)\, e_u \tag{55}$$

Substituting Eq. (32), (37), (39), (45), and (48) into the conservation of energy equation (28), employing ideal gas law, and heats capacity relation, obtaining:

$$E - A_w \left(T_{w,\infty}\, \rho_{\infty,w} \delta_w \left(c_p - c_v \right) - \int_0^p \delta_w \; dp \right)$$

$$- A_{eb} \left(T_{eb,\infty}\, \rho_{\infty,eb} \delta_{eb} \left(c_p - c_v \right) - \int_0^p \delta_{eb} \; dp \right)$$

$$-Q_r + \frac{P\, V_p}{\gamma_u - 1} = \int_0^{m_b} e_b \; dm \; + \; m\,(1 - x_b)\, e_u$$

$$E - A_w \left(p\delta_w - \int_0^p \delta_w \; dp \right) - A_{eb} \left(p\delta_{eb} - \int_0^p \delta_{eb} \; dp \right) - Q_r + \frac{P\, V_p}{\gamma_u - 1} = \int_0^{m_b} e_{b,\infty} \; dm + (1 - x_b)\, m\, e_{u,\infty} \tag{56}$$

Integration by parts could have the form:

$$p\delta - \int_0^p \delta \; dp = \int_0^\delta p \; d\delta' \tag{57}$$

Applying this form into Eq. (50), gives:

$$\frac{E}{m} - \frac{A_w}{m} \left(\int_0^{\delta_w} p \; d\delta' \right) - \frac{A_{eb}}{m} \left(\int_0^{\delta_{eb}} p \; d\delta' \right) - \frac{Q_r}{m} + \frac{P\, V_p}{m\,(\gamma_u - 1)} = \int_0^{m_b} e_{b,\infty} \; dm + (1 - x_b) \; e_{u,\infty} \tag{58}$$

Finally, the conservation equations of specific volume and specific energy, neglecting the terms discussed, can be written as:

$$v_i = \frac{V_c}{m} + \frac{A\, \delta_w}{m} = \int_0^{x_b} v_b \; dx + (1 - x_b)\, v_u \tag{59}$$

$$e_i = \frac{E}{m} - \frac{Q_w + E_w}{m} - \frac{Q_r}{m} = \int_0^{x_b} e_b \; dx + (1 - x_b)\, e_u \tag{60}$$

Where v_i and e_i are representing the initial conditions of the specific volume and the specific energy in the constant volume combustion chamber.

3.6 FORTRAN Code

In the Fortran code calculation, the volume of the electrodes V_e , the displacement volume of the electrode boundary layer V_{eb} , and the displacement volume of the preheat zone V_p , and the conduction energy to the electrodes Q_e are neglected since the changes in these volumes are not affecting the laminar burning speed negatively and without including them would enhance the running process for the Fortran code as well as reducing the converging issues.

The two governing equations Eq. (54) and Eq. (55) are solved to determine the values of the two unknowns; the burned mass fraction x_b and the last layer burned gas temperature $T_b(r,t)$. Then, the pressure is given, as function of time $p\,(t)$, the two governing equations will be solved numerically by introducing the two-dimensional Newton-Raphson method to calculate the burned mass fraction $\dot{x}_b$, as function of time, as well as the temperature distribution in the burned gas region.

3.7 Measurements of Laminar Burning Speed

The flame speed of a fuel is a property which is defined as the expansion of the flame front in a combustible mixture. Flame speed can be classified as either a laminar flame speed or turbulent flame speed and is typically measured in m/s, cm/s, etc. Additionally, flame burning speed has a strong function on such variables as the composition of the mixture, pressure, temperature, equivalence ratios, and diluents. One of the significant purposes for determining a laminar burning speed, it would enhance the engine's efficiency. Moreover, for non-widely used flammable fuels, measuring the flame burning speed with added diluents might be considered beneficial as a working fluid in various systems (i.e. refrigeration systems)

The laminar burning speed could be measured as:

$$s_l = s_f - s_g \tag{61}$$

Where s_l is the laminar burning speed, sg is the unburned gas speed, and s_f is the flame front speed. By propagating a laminar flame radially outward from the vessel center in a constant volume combustion chamber, the laminar burning speed is then defined as:

$$s_l = \frac{\frac{dm_b}{dt}}{\rho_u A_b} = \frac{\dot{m}_b}{\rho_u A_b} = \frac{m\dot{x}_b}{\rho_u A_b} \tag{62}$$

Where m_b is the mass of the burned gas, ρ_u is the gas density of unburned gases, A_b is the area of the burned gas, $\dot{m}_b$ is the burned gas mass rate, m is the total mass of the gas mixture, and $\dot{x}_b$ is the burned gas fraction rate.

Where

$$V_b = \sum v_{bi} m_{bi} = \sum v_{bi}(m x_{bi}) = \frac{4}{3}\,\pi\, r_b^3 - 2\,\pi\, r_e^2 r_b \tag{63}$$

$$A_b = 4\,\pi\, r_b^2 - 2\,\pi\, r_e^2 \tag{64}$$

The second term on the right side is a small value and negligible in order to find the radius of the burned gases as:

$$r_b = \sqrt[3]{\frac{3V_b}{4\pi}} \tag{65}$$

4. Result and Discussion

4.1 Flame Structure and instability

In this thesis, the determination of the flame structures and smoothness can be achieved by the Z-type shadowgraph setup that is utilized a high-speed camera to record the downward flame propagation during combustion. The optical recording of the flame propagation shows the cutoff point where the flame hits the chamber wall as well as the starting point of cellularity developments. The laminar burning speed calculation is obtained based on the assumption that the flame is spherically propagating downward the chamber and cellularity developments are excluded, if appeared. According to the experimental measurements, the cellularity starts to develop at earlier stages at higher pressures and equivalence ratios. One of the observations noticed is that the weak mixtures prevents cellularity to occur at earlier stages.

4.2 Flame Stretch effect

One of the critical considerations implemented for the determination of laminar burning velocities is the negative effect of the stretch effect. Flame stretch occurs by the variation of flame area over time. There are extrapolation calculations have been considered as a zero-stretched laminar flame, however these extrapolations found to be the main sources of discrepancies when compared to other laminar burning speed data. Zero-stretched laminar flame is extremely hard to be achieved but rather a negligible-stretched laminar flame can be acquired by excluding the early burning speed data along the isentropic curve. For spherically downward expanding flames stretch rate is defined as:

$$K = \frac{1}{A}\frac{dA}{dt} = \frac{2}{r}\frac{dr}{dt}$$

In order to investigate the stretch effect on laminar burning speeds, a set of various experiments have been studied over a wide range of different initial temperatures along with its corresponding initial pressures that is seen in the isentropic curve shown in Figure 13. As clearly can be seen that the stretch effect is a strong function of the flame radius, the higher flame radius the less stretch rates. The selected conditions are at initial temperatures of 300, 320, 340, and 360 K each of which has its corresponding initial pressures obtained by the isentropic curve with fixed equivalence ratio of 1 as shown in Figure 13. A-A' represents the first selected condition of a room temperature and an atmospheric pressure. B-B' represents the second selected condition of an initial temperature of 320 K and initial pressure of 1.30 atm. C-C' shows the next selected condition of an initial temperature of 340 K and initial pressure of 1.62 atm. D-D' shows the tested condition of an initial temperature of 360 K and an initial pressure of 2.04 atm. E demonstrates the shared point for the four tested conditions. These measurements are on a single isentropic curve. These tested conditions have different initial conditions, they obviously will have different radii, and therefore the laminar burning speed date will be evaluated and analyzed at various stretch rates. Figure 14 shows the negligible variations of laminar burning speeds along with the stretch rate at equivalence ratio of 1.0 for the selected case of temperature of 420 K and corresponding pressure of 3.71 atm. According to the result, the variations of the laminar burning speeds can be negligible. Additionally, the experimental results show that the laminar burning speed at a flame radius larger than 4cm has negligible stretch rates. Also, measurements can be only collected for when the flame radius between 4cm and 8cm where the flame reaches to the chamber wall. These restrictions can be maintained by the high-speed camera to verify the flame characteristics and flame smoothness as burning speed measurements were only restricted to smooth flames.

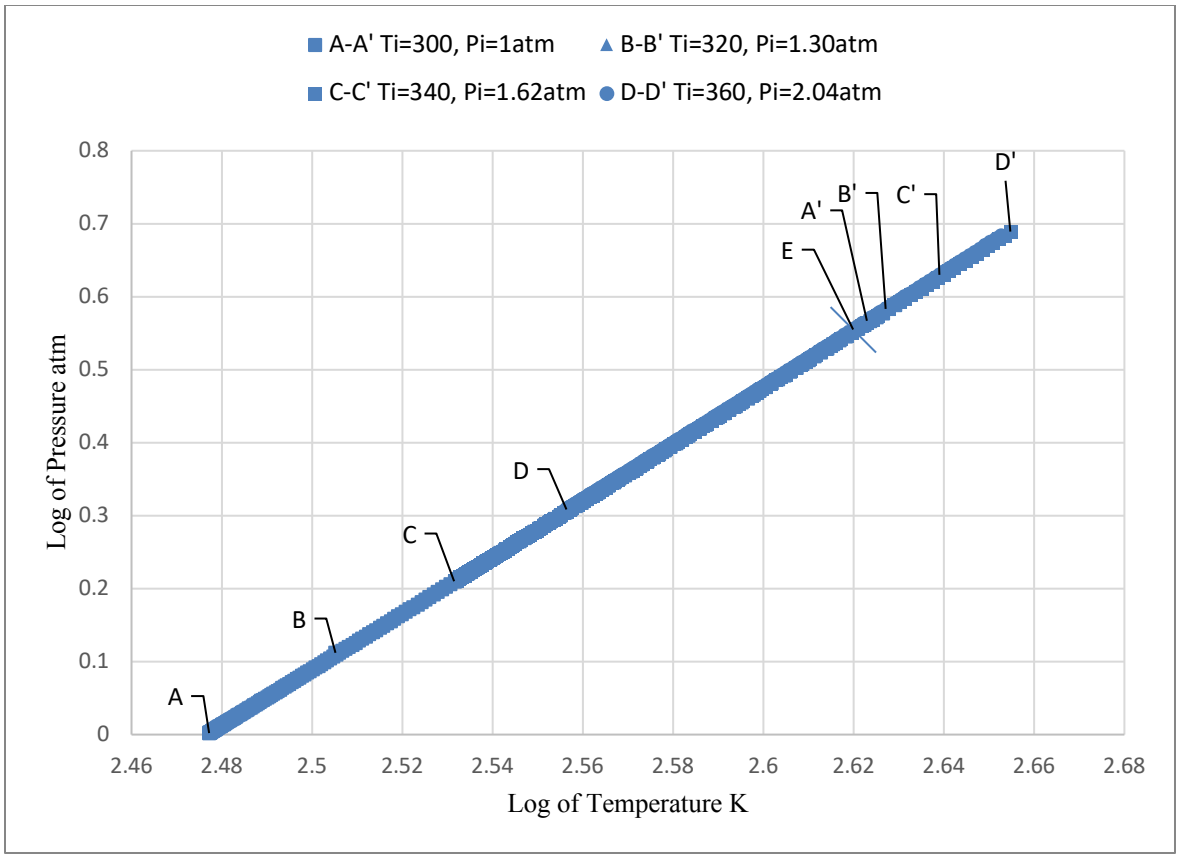

Figure 13: Various starting conditions of four different experiments selected in a way to be joined along the isentropic curve, E represents the selected case.

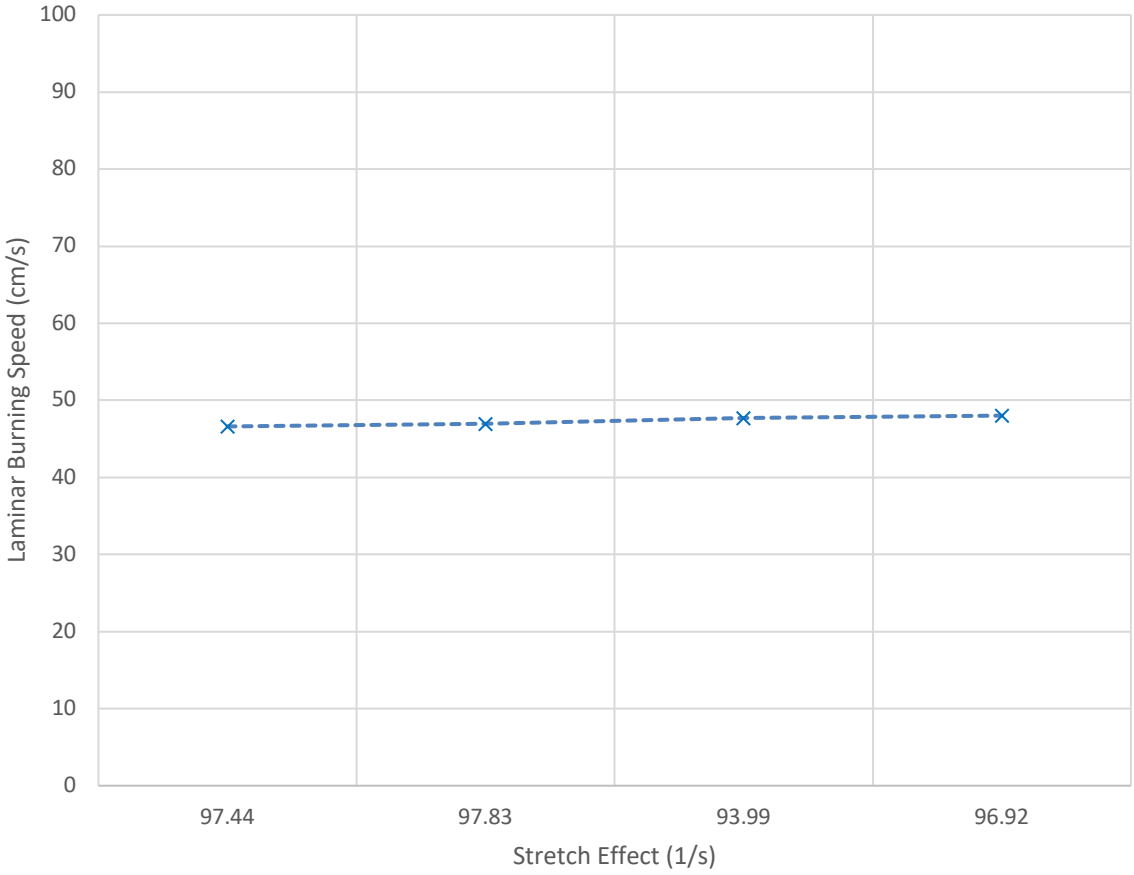

Figure 14: Four different selected data shows a negligible variation of burning speeds all of which at a temperature of 420 K and pressure of 3.71 atm.

The laminar burning speeds of mixtures of propane-air (C_3H_8) and a wide range of additional carbon dioxide (CO_2) concentrations at various equivalence ratios ranging from 0.80 to 1.20, and pressures of 0.50 to 4 atm, and elevated temperatures of 400 K to 600 K have been measured. The selected carbon dioxide (CO_2) concentrations are 20%, 40%, 60%, 80% as well as the pure propane-air (C_3H_8). The experimental work has been carried out for 94 different cases. The pure propane-air (C_3H_8) is selected to have an overview on how the additional carbon dioxide (CO_2) reacts and decreases the laminar burning speeds. As the activation of chemical reactions occur by temperature, it was clearly observed that the burning speed increases with the higher temperatures and more importantly decreases with higher pressures. In additions, the laminar burning speeds increase as the fuel-air ratios increase from lean mixture of 0.80 ratio to reach mixture of 1.20.

Laminar burning speed of experiments with initial temperature of 400 K

The laminar burning speeds for different air-fuel ratio is highly dependent on the carbon dioxide (CO_2) concentrations. According to Figure 15, for pure propane-air (C_3H_8) laminar burning speeds at rich mixture are faster than both the stoichiometric and the lean mixture. Also, a repeated trend has been observed in the atmospheric pressure case with lower burning speeds as seen in Figure 16. For higher initial pressure of 2 atm, the burning speeds are slower as the pressure increased, however the collected data were restricted before cellularity development starts at earlier stages and this will reduce the collected laminar burning speed data as seen in Figure 17.

For 20% of carbon dioxide diluent, the laminar burning speeds have been lowered since the carbon dioxide is non-flammable gas, as shown in Figure 18. For the same carbon dioxide concentration at atmospheric pressure, the laminar burning speeds have been reduced upon the increasing of the initial pressure as shown in Figure 19, compared to 0.50 atm. In addition, Figure 20 shows the lowest measured burning speeds for the 20% of carbon dioxide diluent at a higher initial pressure of 2 atm.

For 40% of carbon dioxide concentrations, the burning speeds have been minimized and the fuel-air ratio of 1.20 is still faster than the stoichiometric, as seen in Figure 21. For atmospheric initial pressure, the laminar burning speeds have been decreased as the initial pressure increased from 0.50 to 1 atm as noticed in Figure 22. Moreover, Figure 23 demonstrates a lower burning speeds at a higher initial pressure of 2 atm, however, the cellularity development starts at earlier stages.

For 60% of carbon dioxide concentrations, the added carbon dioxide concentration has lowered the laminar burning speeds and a shift of the fuel-air ratio is experimentally observed according to Figure 24. This shift is because of the flame peak adiabatic flame temperature decreases as the addition of carbon dioxide diluent increased. According to Figure 25, the fuel-air ratio of 1 is faster than the rich mixture for the case of initial pressure of 0.5 atm. Figure 26 demonstrates a lower burning speeds at a higher initial pressure of 2 atm for the same concentration of carbon dioxide.

A similar trend has been noticed for the case of 80% of carbon dioxide diluent in terms of the equivalence ratio according to Figure 27. The stoichiometric ratio as seen in Figure 28 is faster than the equivalence ratio of 1.2 as the peak adiabatic flame temperature shifts and this will be discussed in detail using STANJAN software. The burning speeds of mixtures of propane-air (C_3H_8) and additional of 80% of carbon dioxide (CO_2) diluent have been measured at only initial pressures of 1 and 2 atm since the flame could not be generated at 0.50 atm.

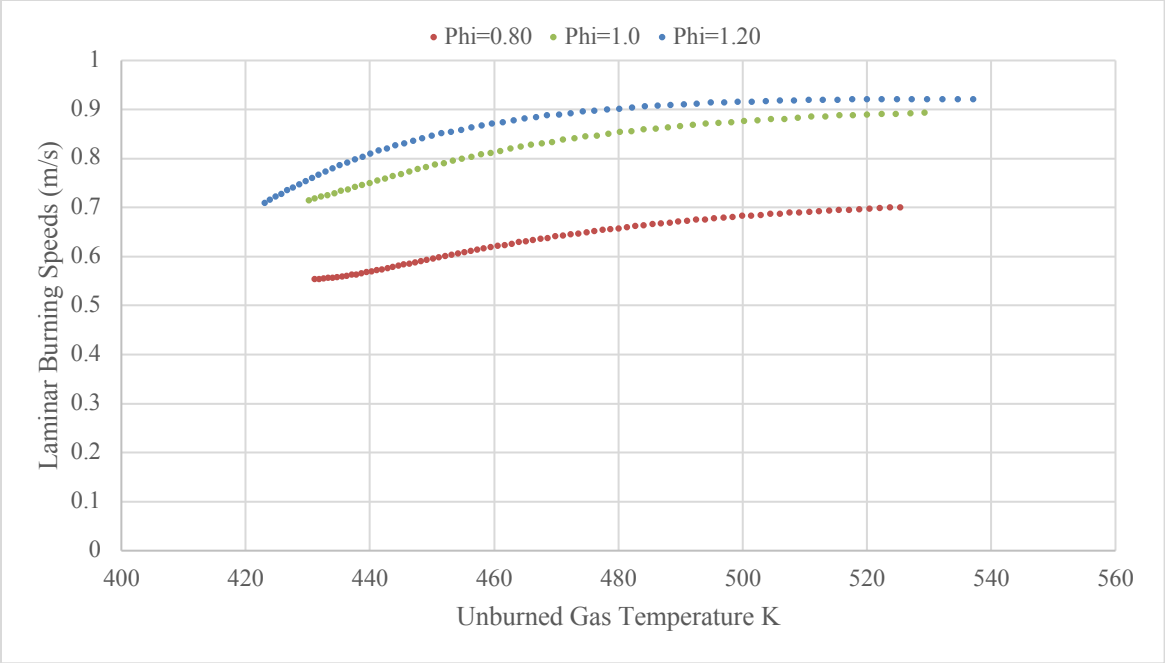

Figure 15: Laminar burning speeds for pure propane at P_i = 0.50 atm, T_i = 400 K and different equivalence ratios 0.80,1.0,1.20

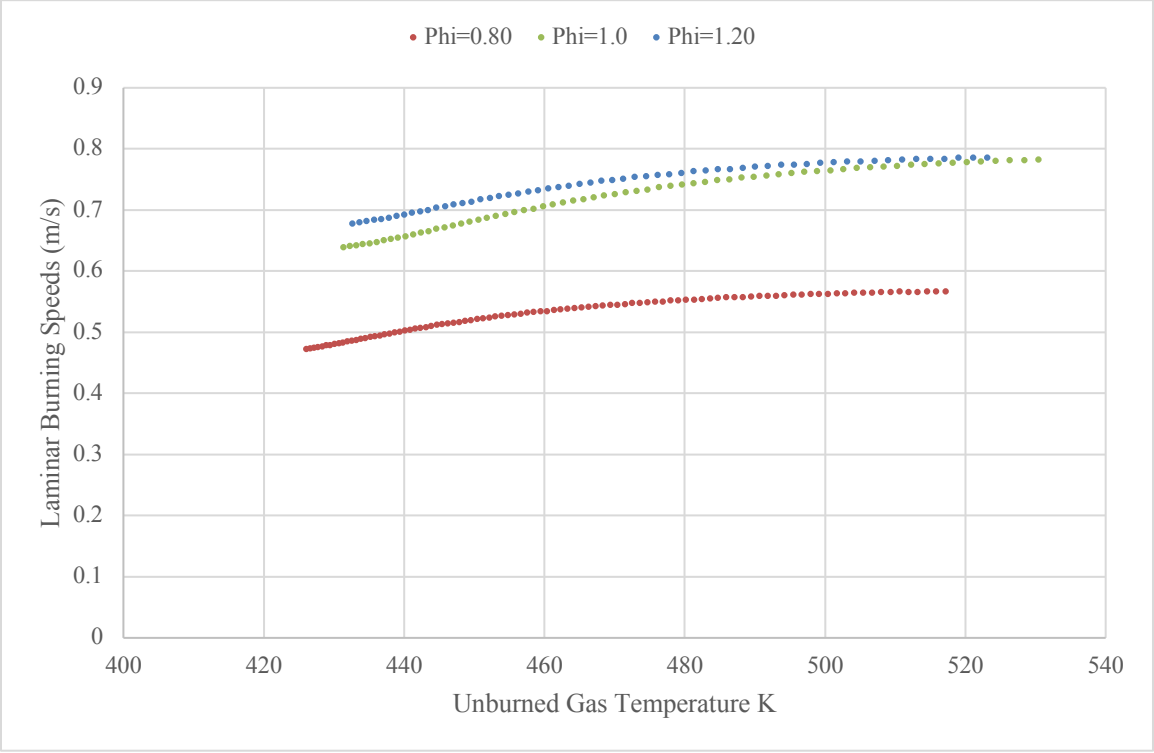

Figure 16: Laminar burning speeds for pure propane at P_i = 1 atm, T_i = 400 K and different equivalence ratios 0.80,1.0,1.20

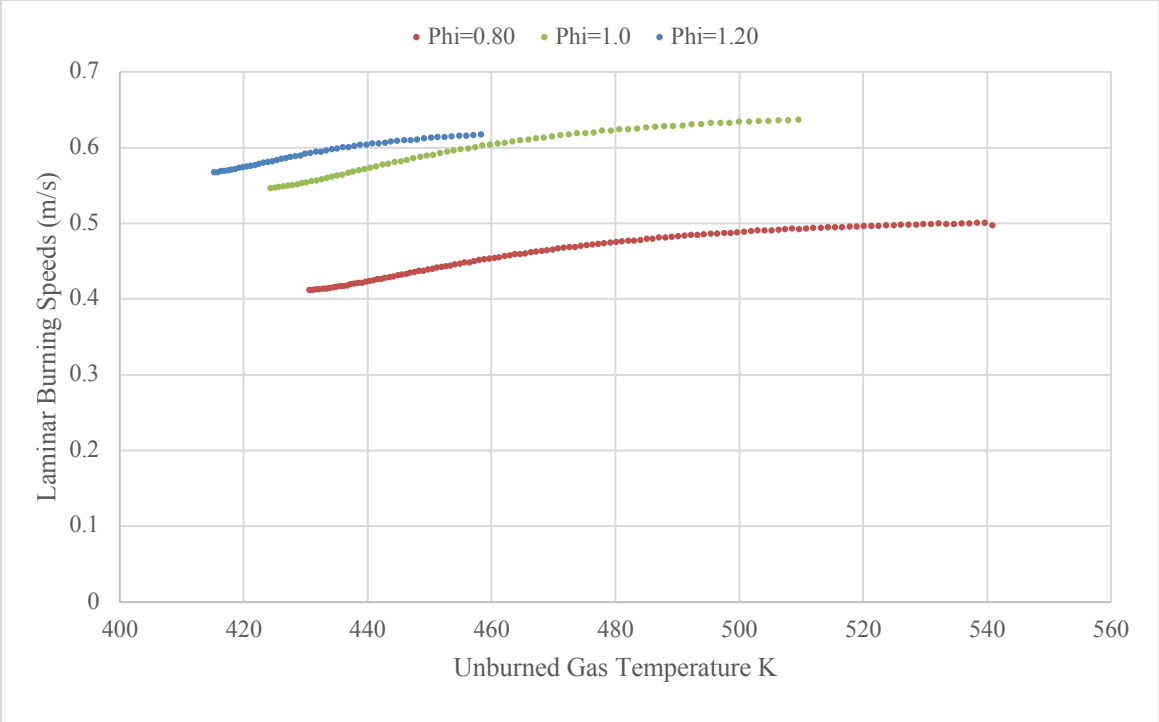

Figure 17: Laminar burning speeds for pure propane at P_i = 2 atm, T_i = 400 K and different equivalence ratios 0.80,1.0,1.20

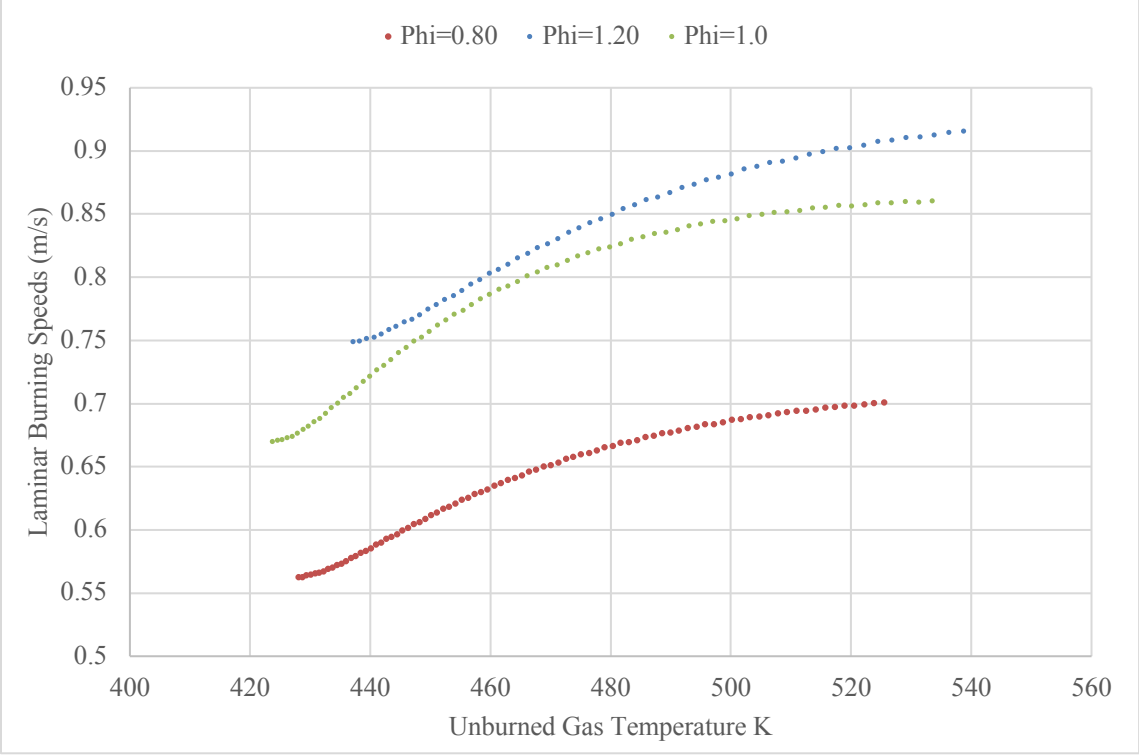

Figure 18: Laminar burning speeds for propane and 20% of carbon dioxide at P_i = 0.50 atm, T_i = 400 K and different equivalence ratios 0.80,1.0,1.20

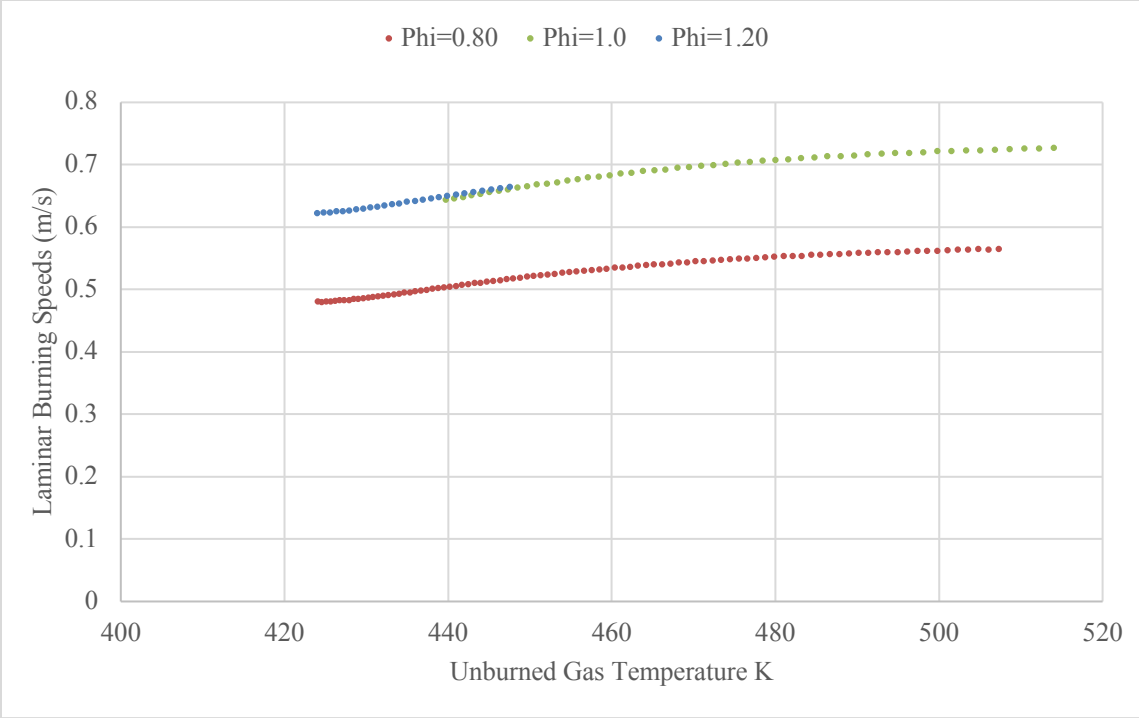

Figure 19: Laminar burning speeds for propane and 20% of carbon dioxide at P_i = 1 atm T_i = 400 K and different equivalence ratios 0.80,1.0,1.20

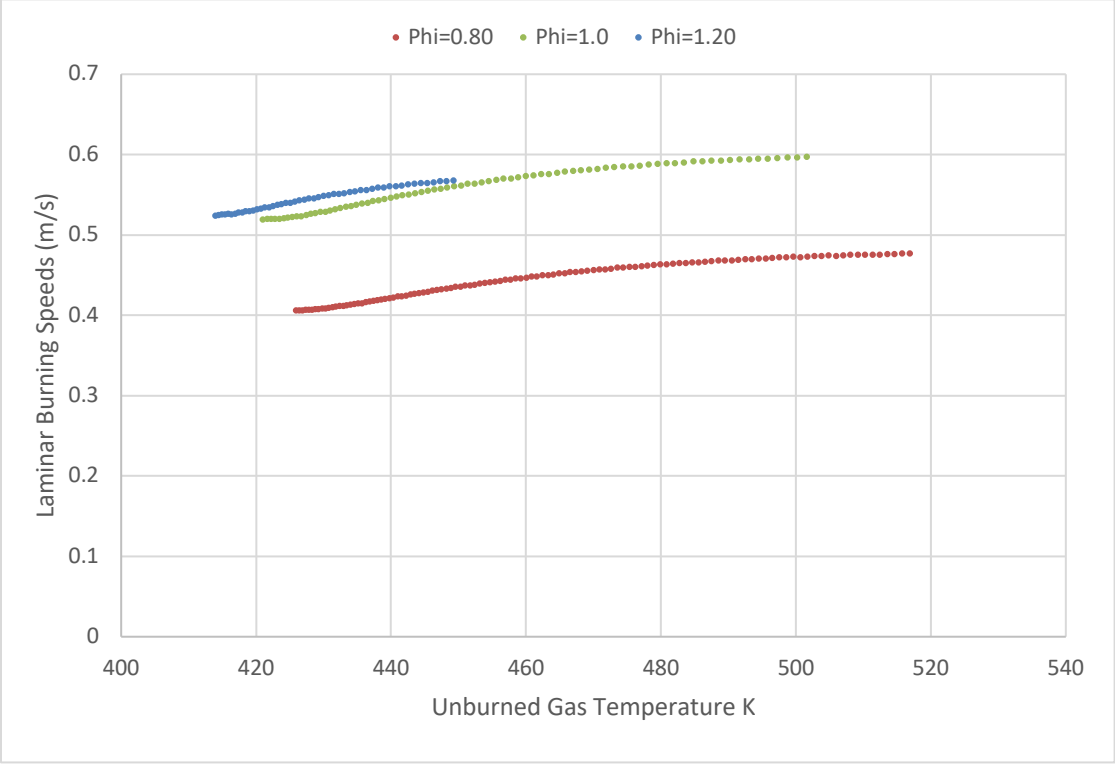

Figure 20: Laminar burning speeds for propane and 20% of carbon dioxide at P_i = 2 atm T_i = 400 K and different equivalence ratios 0.80,1.0,1.20

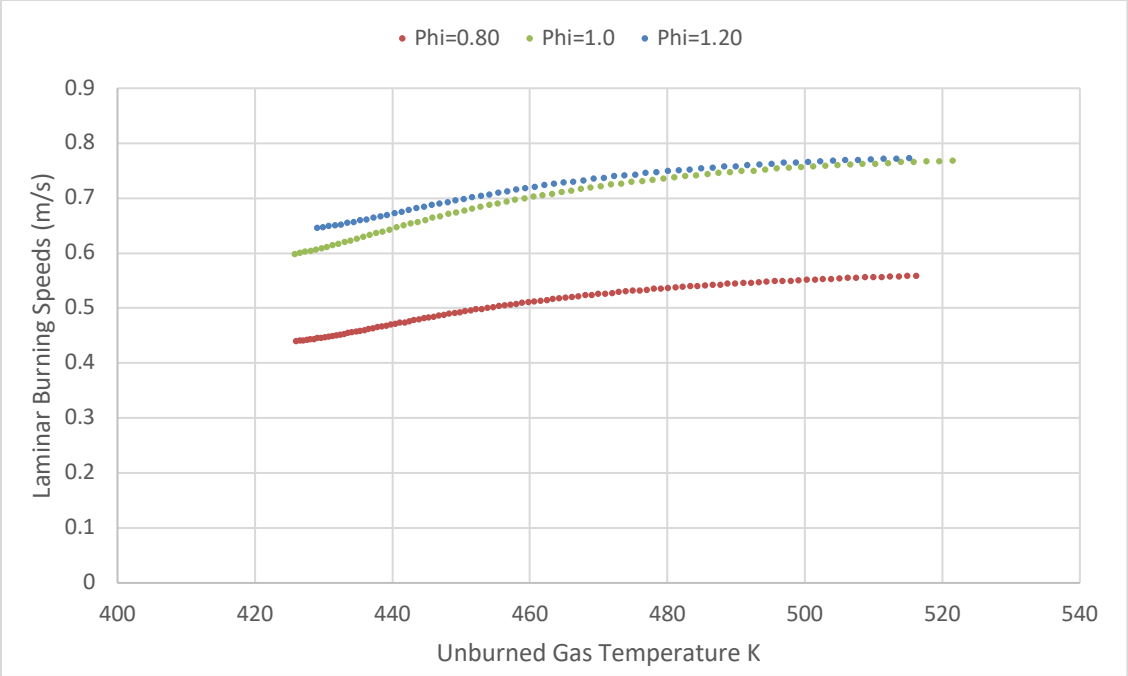

Figure 21: Laminar burning speeds for propane and 40% of carbon dioxide at P_i = 0.50 atm, T_i = 400 K and different equivalence ratios 0.80,1.0,1.20

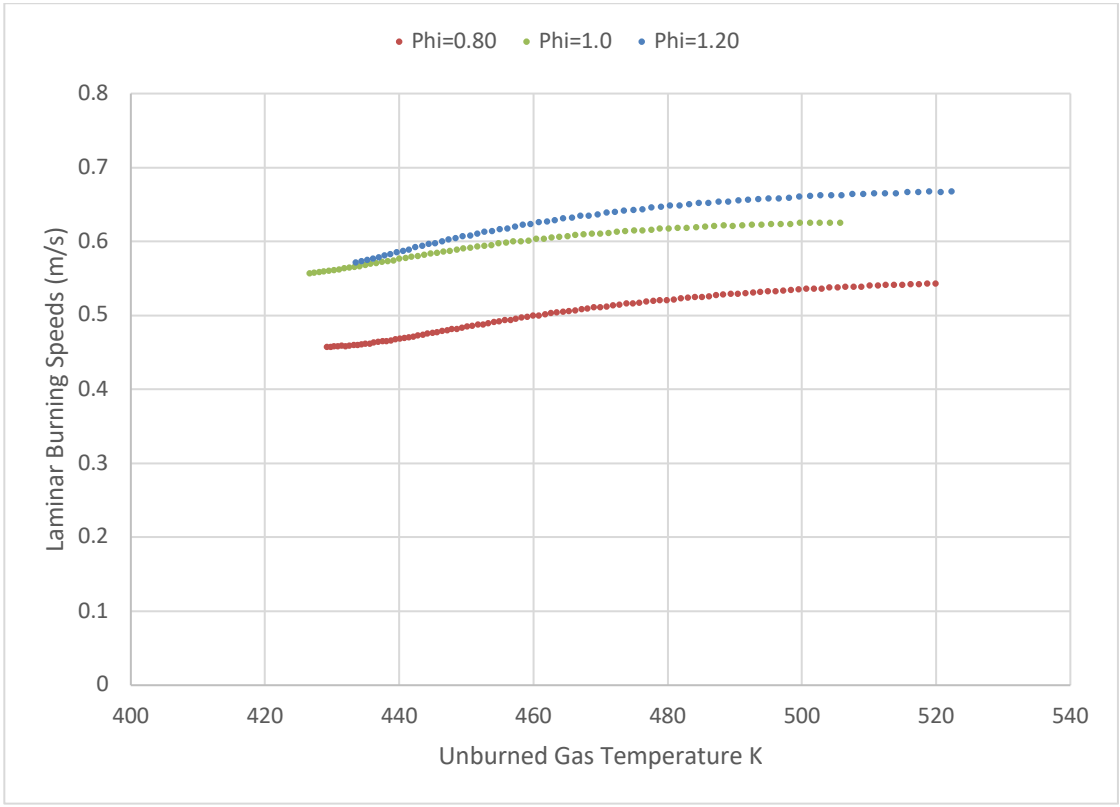

Figure 22: Laminar burning speeds for propane and 40% of carbon dioxide at P_i = 1 atm T_i = 400 K and different equivalence ratios 0.80,1.0,1.20

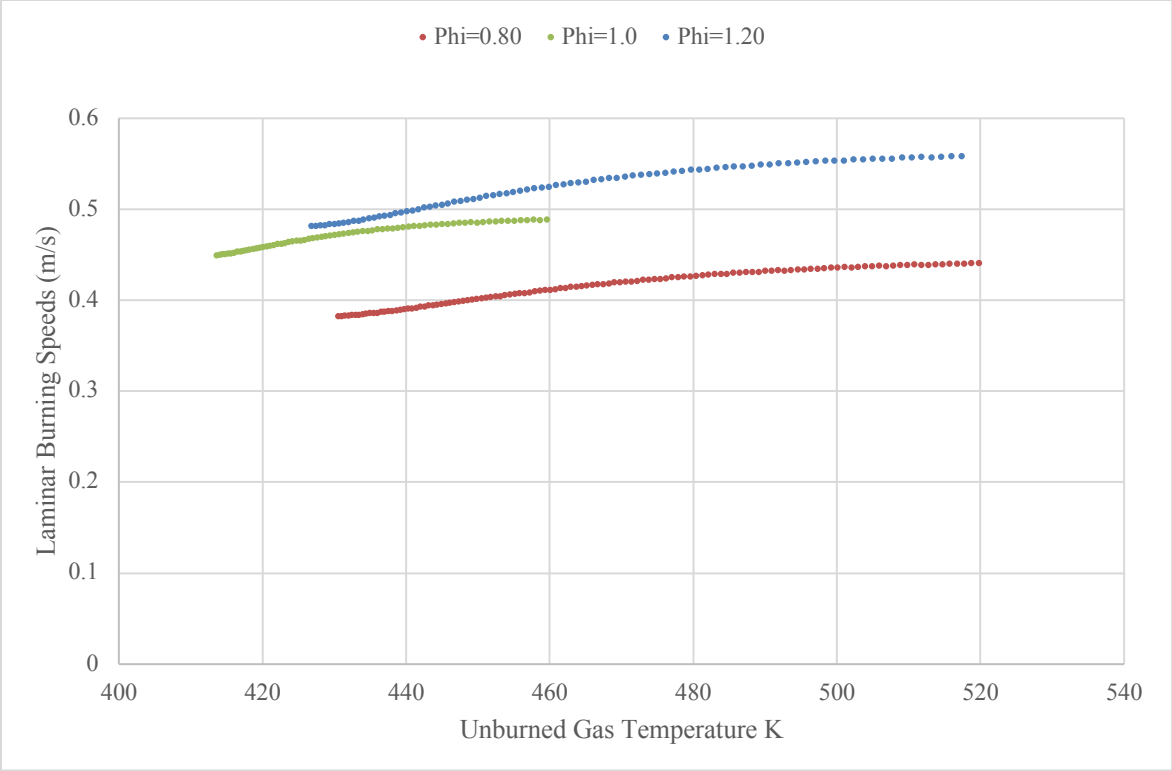

Figure 23: Laminar burning speeds for propane and 40% of carbon dioxide at P_i = 2 atm, T_i = 400 K and different equivalence ratios 0.80,1.0,1.20

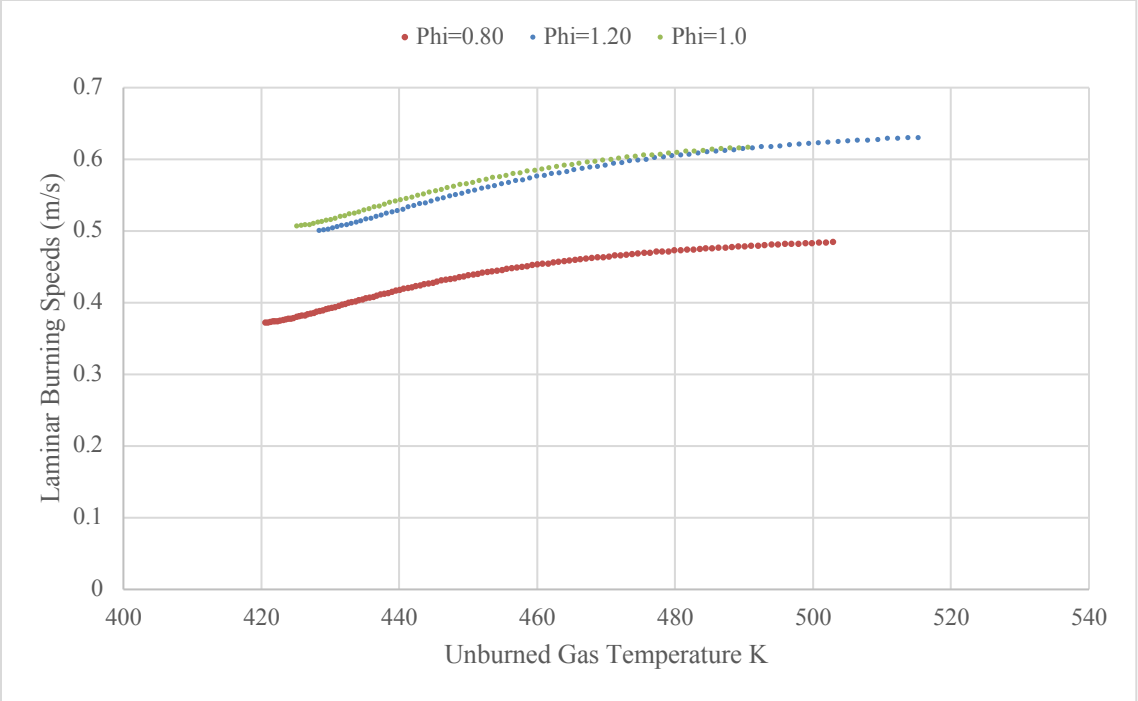

Figure 24: Laminar burning speeds for propane and 60% of carbon dioxide at P_i = 0.50 atm, T_i = 400 K and different equivalence ratios 0.80,1.0,1.20

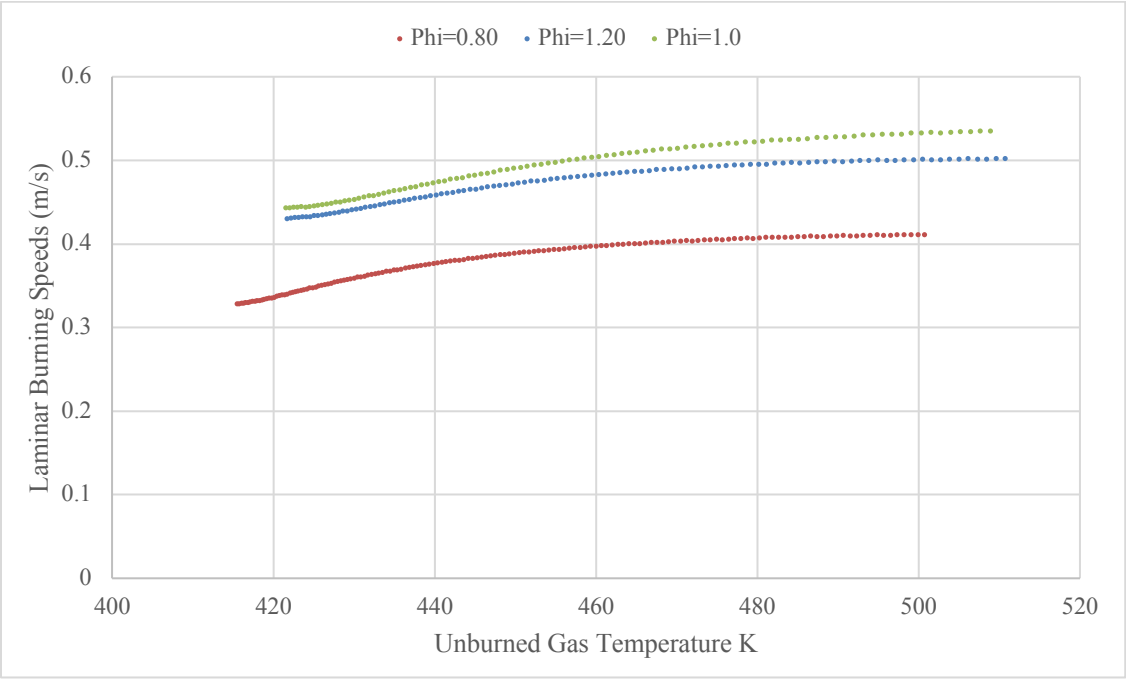

Figure 25: Laminar burning speeds for propane and 60% of carbon dioxide at P_i = 1 atm, T_i = 400 K and different equivalence ratios 0.80,1.0,1.20

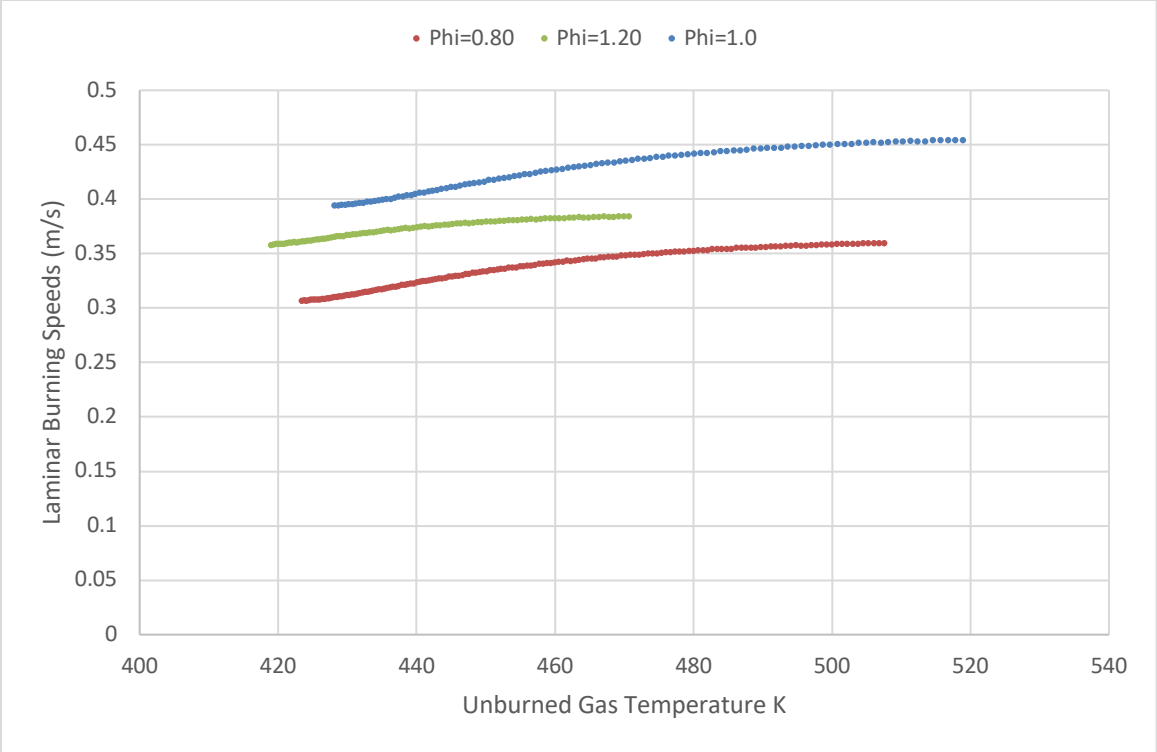

Figure 26: Laminar burning speeds for propane and 60% of carbon dioxide at P_i = 2 atm T_i = 400 K and different equivalence ratios 0.80,1.0,1.20

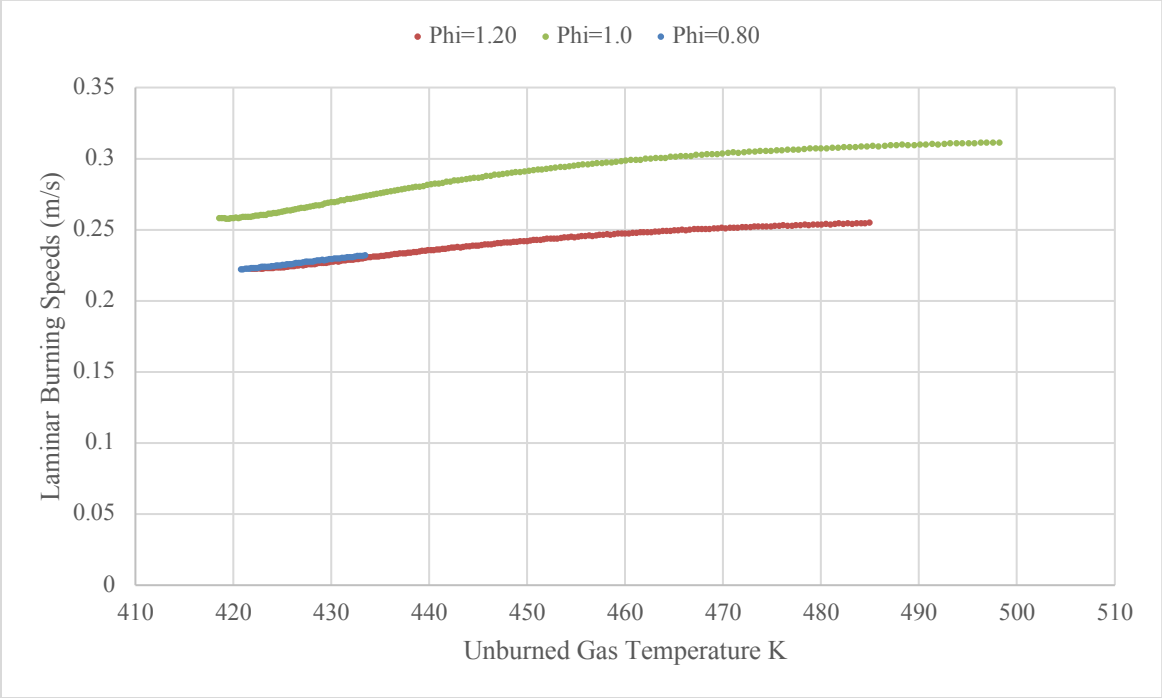

Figure 27: Laminar burning speeds for propane and 80% of carbon dioxide at P_i = 1 atm T_i = 400 K and different equivalence ratios 0.80,1.0,1.20

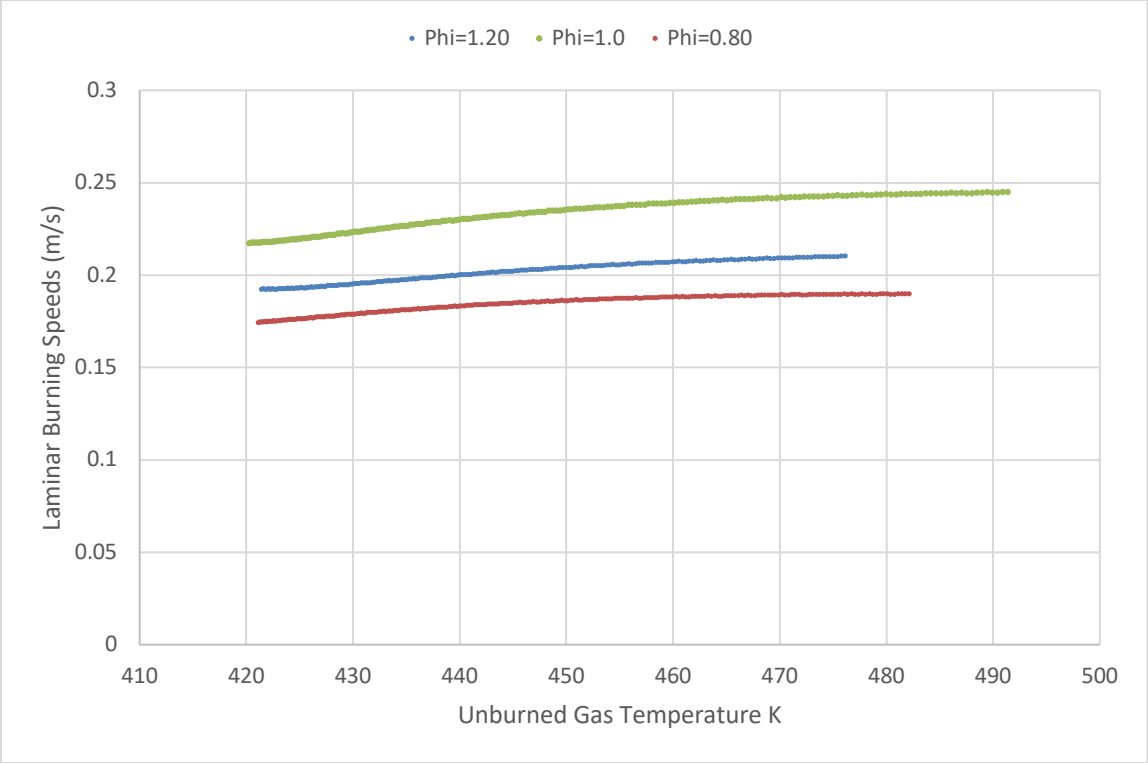

Figure 28: Laminar burning speeds for propane and 80% of carbon dioxide at P_i = 2 atm, T_i = 400 K and different equivalence ratios 0.80,1.0,1.20

Laminar burning speed of experiments with initial temperature of 480 K

The result of laminar burning speeds with initial temperature of 480 K shows overall higher laminar burning speeds than that of initial temperature of 400 K. The pure propane-air (C_3H_8) at rich mixture is faster than lean as well as stoichiometric mixtures as seen in Figure 29. Moreover, similar trend has been observed but with lower burning speeds in the case of the atmospheric initial pressure as shown in Figure 30. For higher initial pressure of 2 atm, the initial pressure has been raised and this will certainly reduce laminar burning speeds as seen in Figure 31. However, the number of the collected data are less since cellularity will develop at earlier stages and this will negatively reduce the collected data as these measurements were only for smooth flame.

For 20% of carbon dioxide diluent, the laminar burning speeds have been reduced and burning speeds of fuel-air ratio of 1.20 is faster among the other two fuel-air ratios as shown in Figure 32. Also, at the atmospheric initial pressure, the rich mixture shows higher laminar burning speeds than the fuel-air ratio of 0.80 and 1 but the overall burning speeds are lower compared to 0.5 atm, as seen in Figure 33. According to Figure 34, cellularity development is reduced greatly by lowering the equivalence ratios for elevated initial pressure.

For the addition of carbon dioxide concentrations to 40%, the burning speeds have been decreased, and in a similar way as the previous tests, the obtained data illustrates higher burning speeds at fuel-air ratio of 1.20 than the stoichiometric, as demonstrated in Figure 35. As the initial pressure increased to atmospheric, the laminar burning speeds lowered and the trend of the different fuel-air ratios remains the same that the rich mixture has higher burning speed rates as shown in Figure 36. For elevated initial pressure, the lower equivalence ratio prevents cellularity development to begin and in that way the collected data of lean and stoichiometric mixtures are more than the collected data of rich mixture as noticed in Figure 37.

In the 60% of carbon dioxide concentrations, the blends at the stoichiometric ratio shows a rapid burning speeds than the rich and this is usually as the peak adiabatic flame temperature approaches to the lean mixture as noticed in Figure 38. According to Figure 39, lowered burning speeds have been noticed as the initial pressure increased from 0.50 to 1 atm. For initial pressure of 2 atm, overall slower laminar burning speeds have been observed in the fuel-air ratios of 0.80 to 1.20 and higher cellularity developments started but were not included in the analysis since the conducted measurements requires the flame to be smooth as demonstrated in Figure 40.

In terms of the fuel-air ratios, similar behavior of 60% of carbon dioxide was observed for the 80% of carbon dioxide concentration. At atmospheric initial pressure, the burning speeds of stoichiometric ratio is faster than both the rich and the lean mixtures as seen in Figure 41. Moreover, the burning speeds at a higher initial pressure are reduced greatly upon mixing of the 80% carbon dioxide diluent, according to Figure 42.

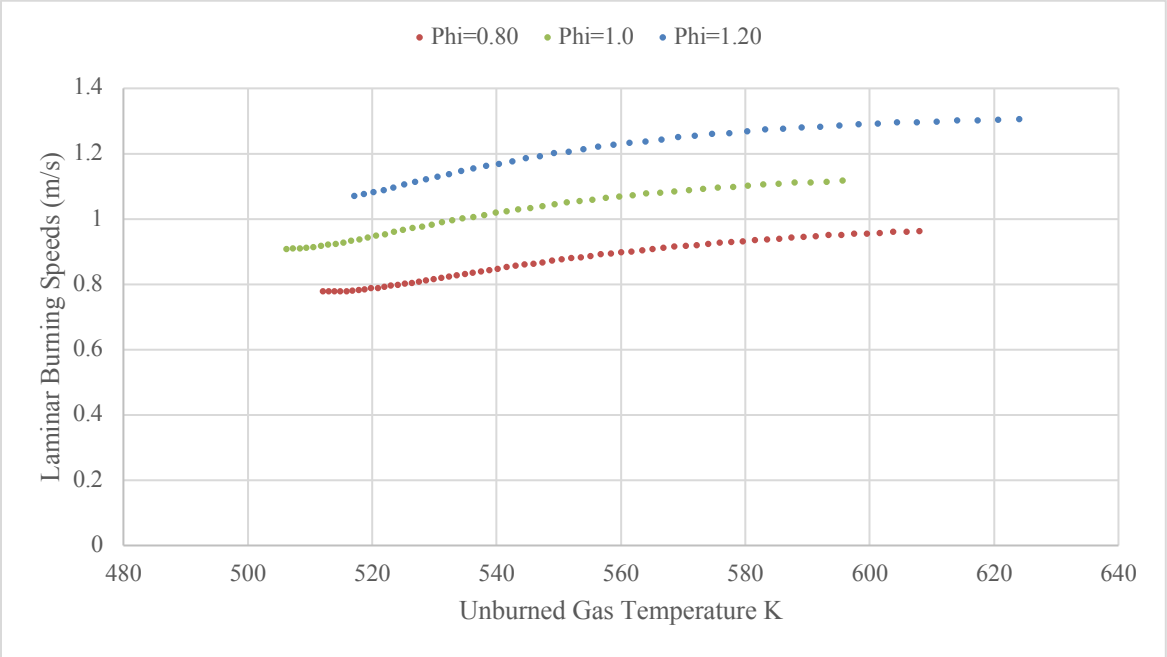

Figure 29: Laminar burning speeds for pure propane at P_i = 0.50 atm, T_i = 480 K and different equivalence ratios 0.80,1.0,1.20

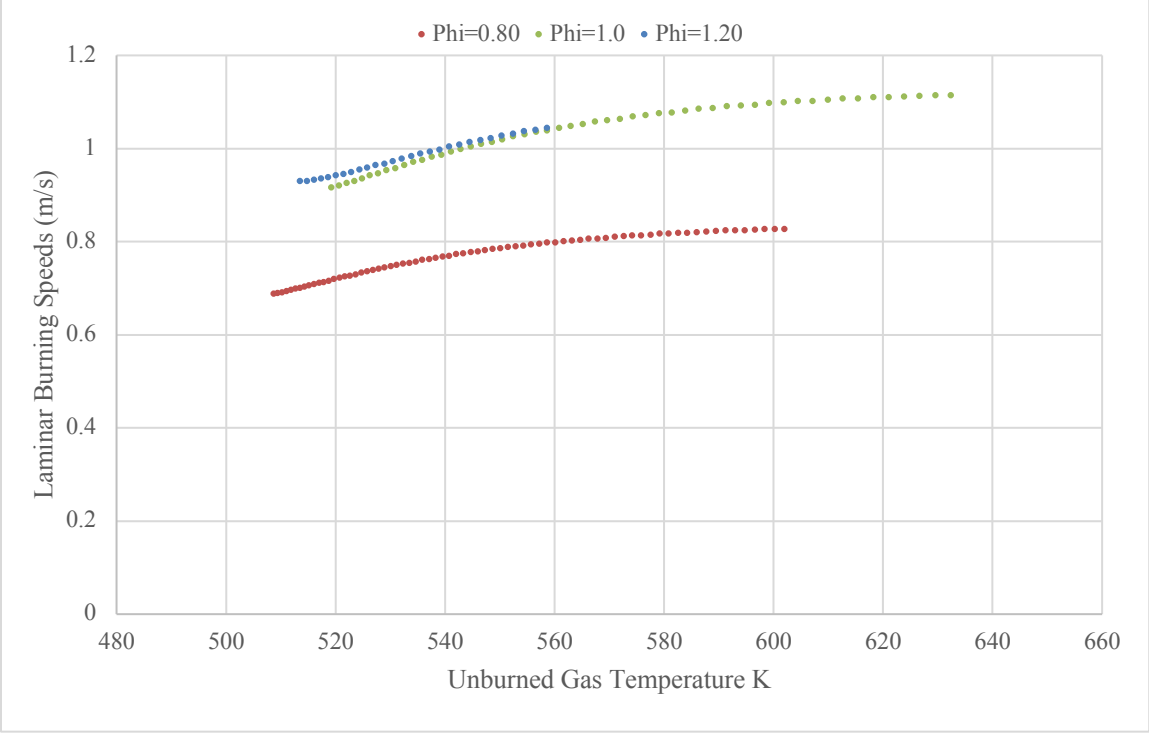

Figure 30: Laminar burning speeds for pure propane at P_i = 1atm, T_i = 480 K, and different equivalence ratios 0.80,1.0,1.20

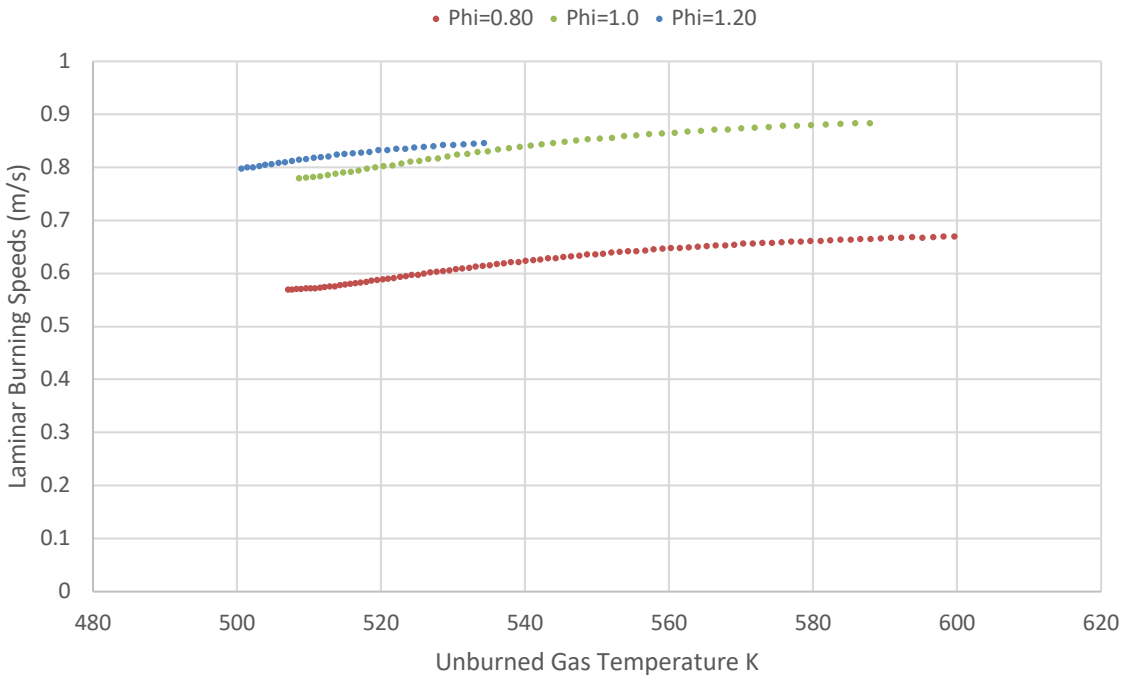

Figure 31: Laminar burning speeds for pure propane at P_i = 2 atm, T_i = 480 K different equivalence ratios 0.80,1.0,1.20

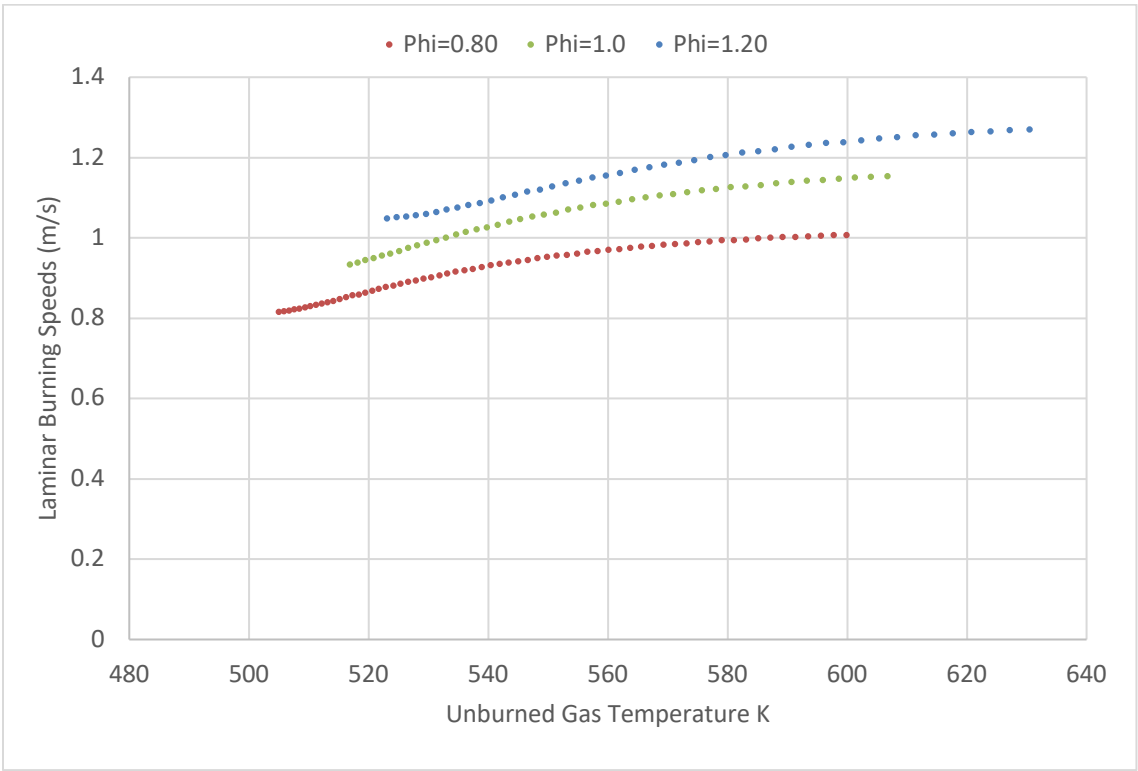

Figure 32: Laminar burning speeds for propane and 20% of carbon dioxide at P_i = 0.5 atm , T_i = 480 K and different equivalence ratios

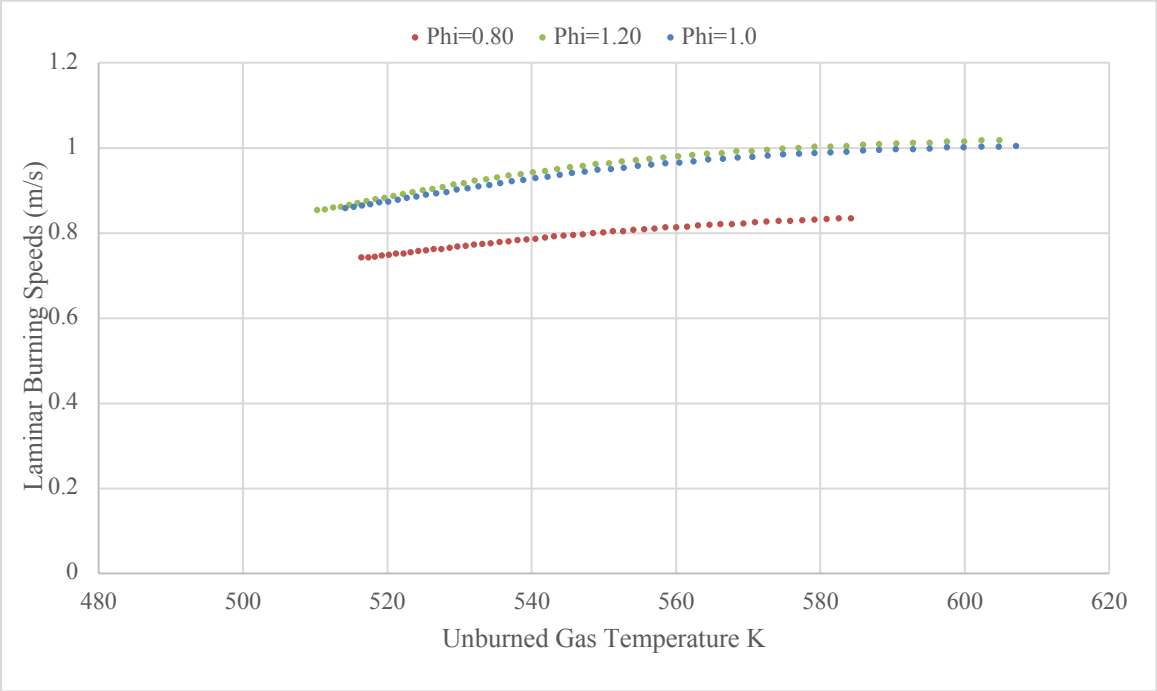

Figure 33: Laminar burning speeds for propane and 20% of carbon dioxide at P_i = 1 atm, T_i = 480 K and different equivalence ratios

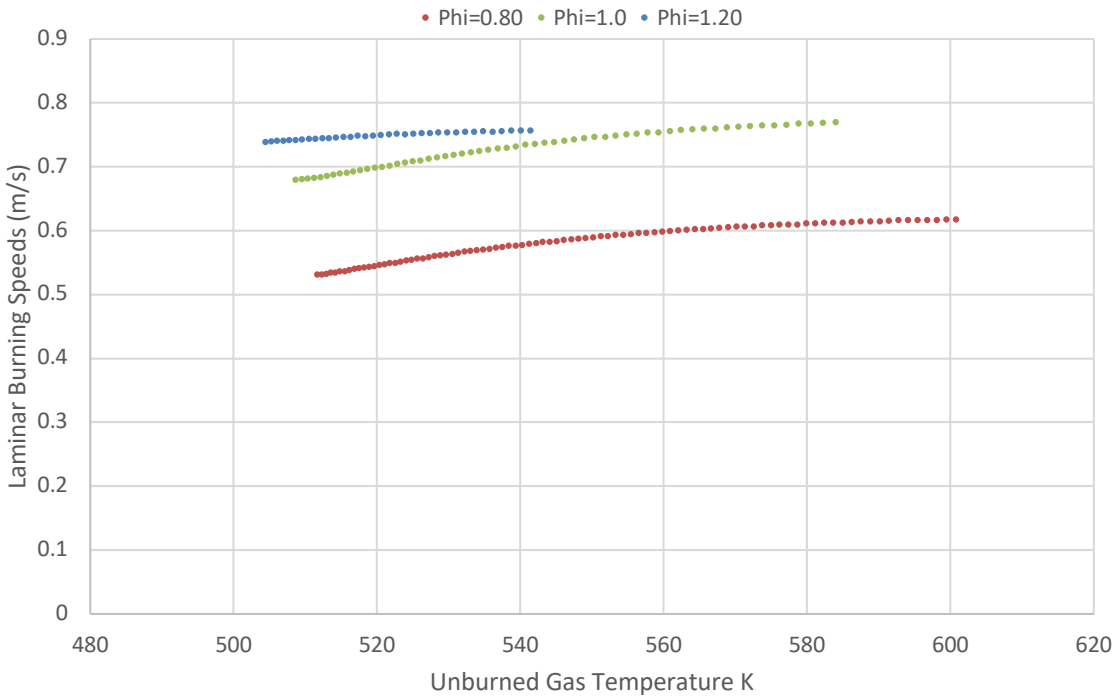

Figure 34: Laminar burning speeds for propane and 20% of carbon dioxide at P_i = 2 atm, T_i = 480 K and different equivalence ratios

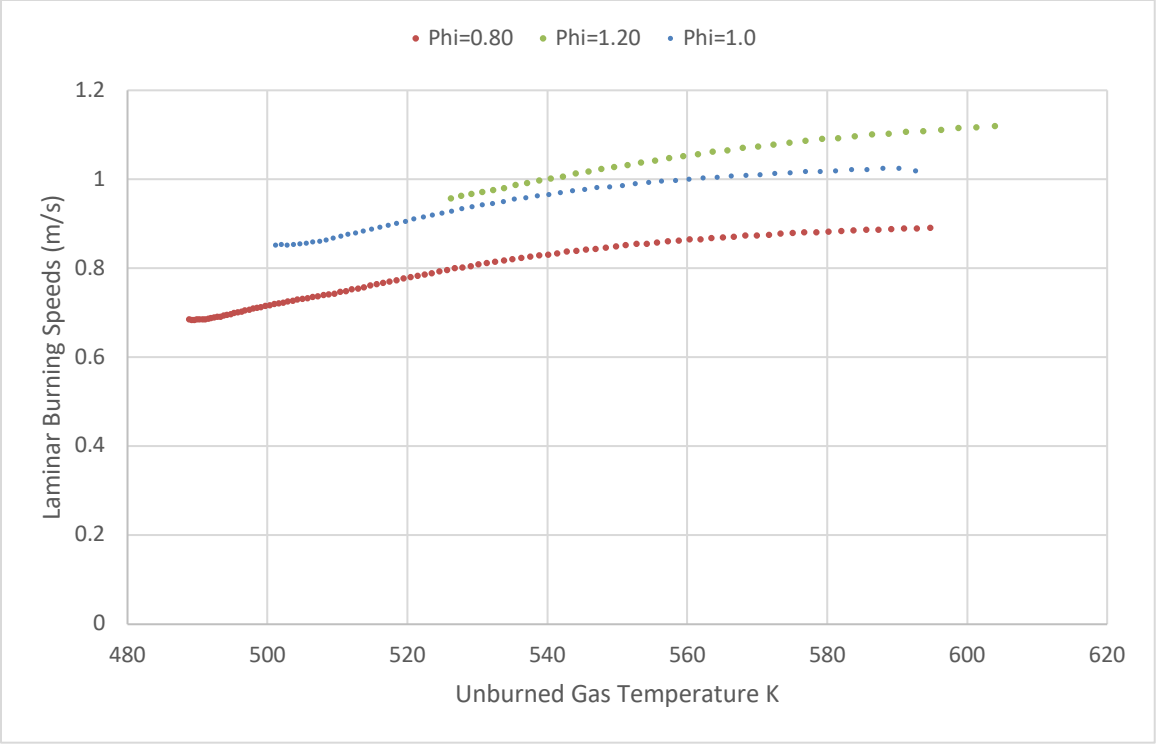

Figure 35: Laminar burning speeds for propane and 40% of carbon dioxide at P_i = 0.50 atm, T_i = 480 K and different equivalence ratios

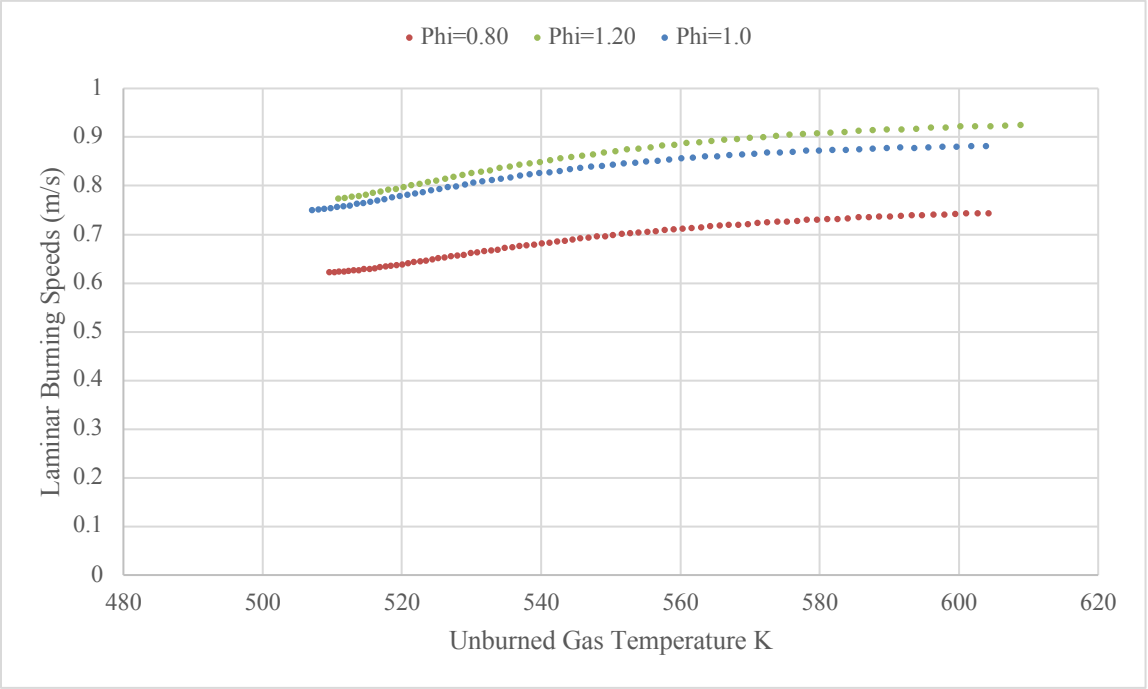

Figure 36: Laminar burning speeds for propane and 40% of carbon dioxide at P_i = 1 atm, T_i = 480 K and different equivalence ratios

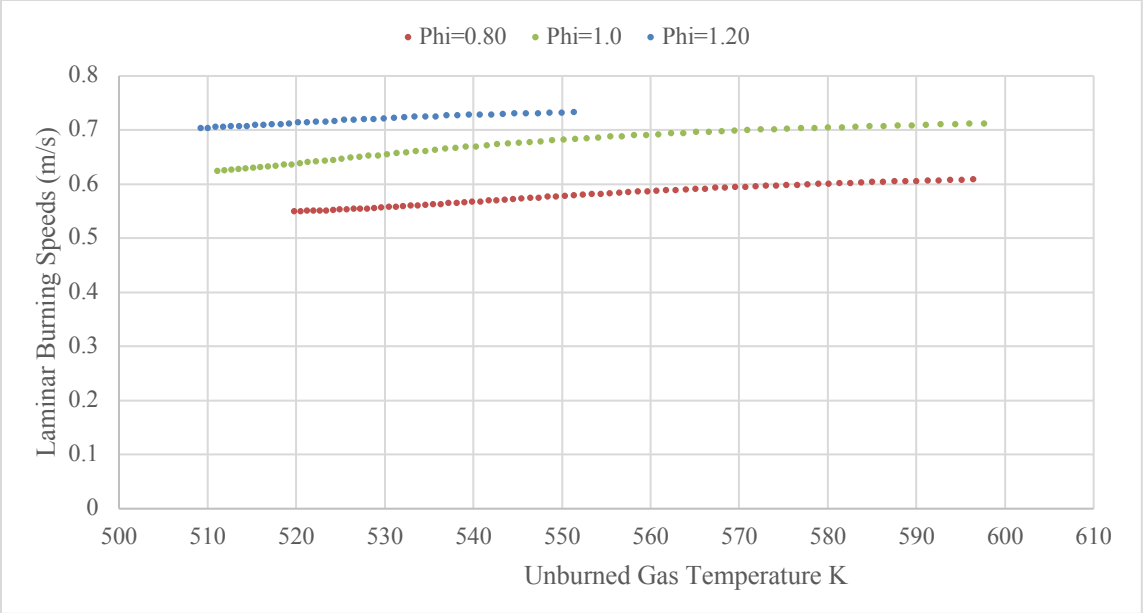

Figure 37: Laminar burning speeds for propane and 40% of carbon dioxide at P_i = 2 atm, T_i = 480 K different equivalence ratios

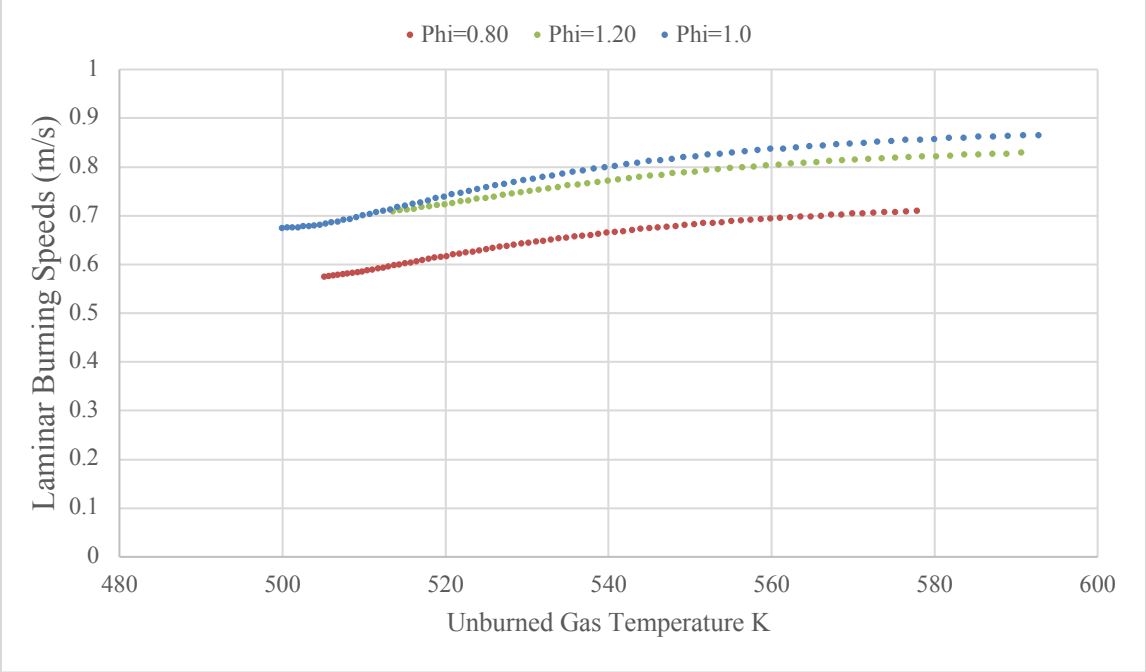

Figure 38: Laminar burning speeds for propane and 60% of carbon dioxide at P_i = 0.50 atm, T_i = 480 K and different equivalence ratios

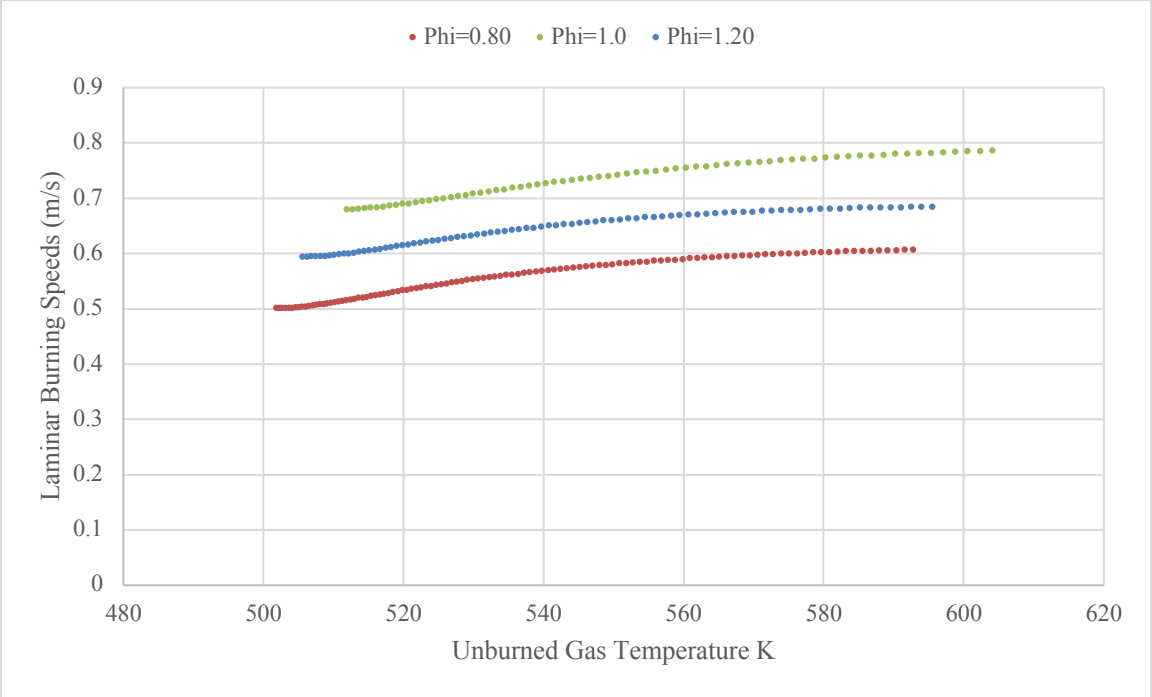

Figure 39: Laminar burning speed for propane and 60% of carbon dioxide at P_i = 1 atm, T_i = 480 K and different equivalence ratios

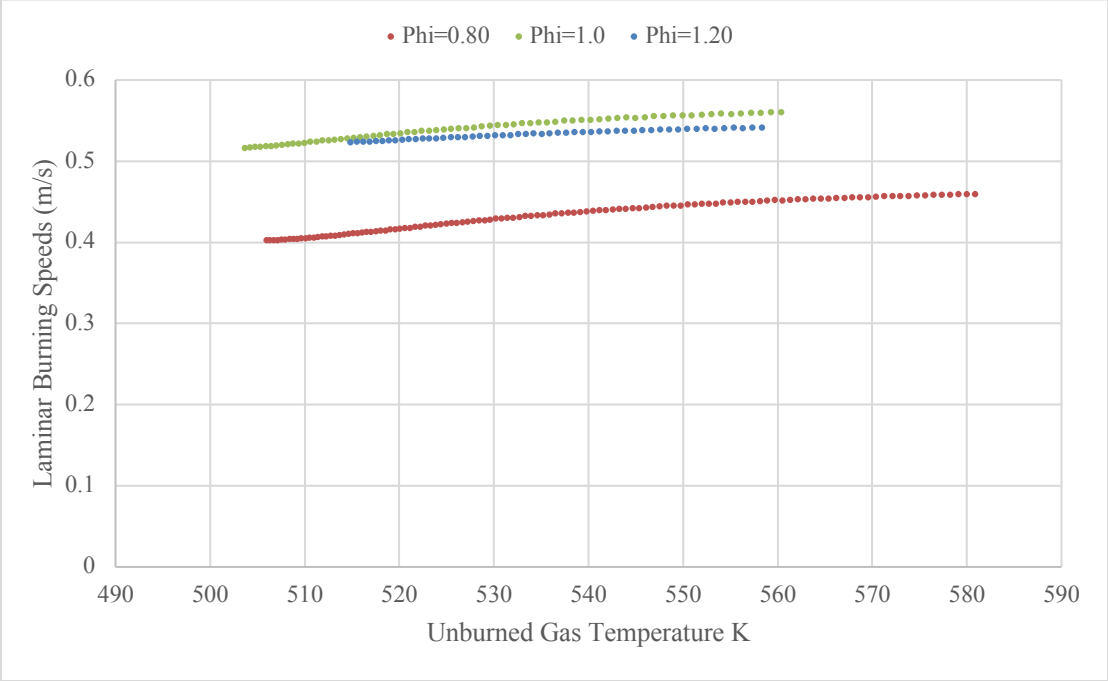

Figure 40: Laminar burning speeds for propane and 60% of carbon dioxide at P_i = 2 atm, T_i = 480 K different equivalence ratios

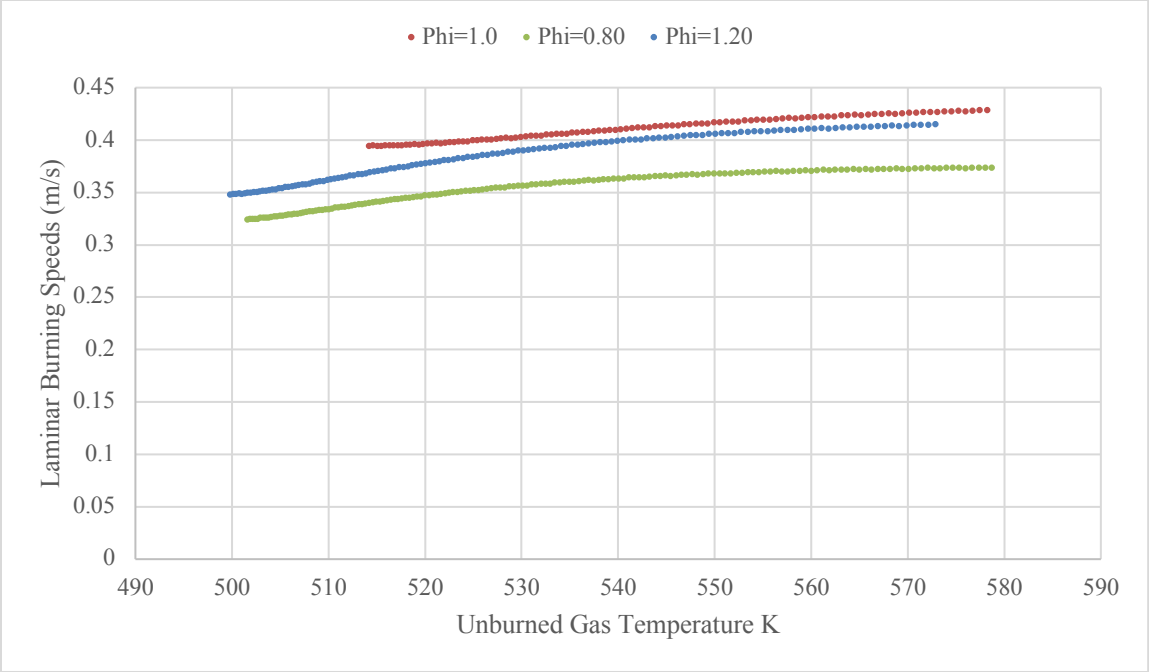

Figure 41: Laminar burning speeds for propane and 80% of carbon dioxide at P_i = 1 atm, T_i = 480 K and different equivalence ratios

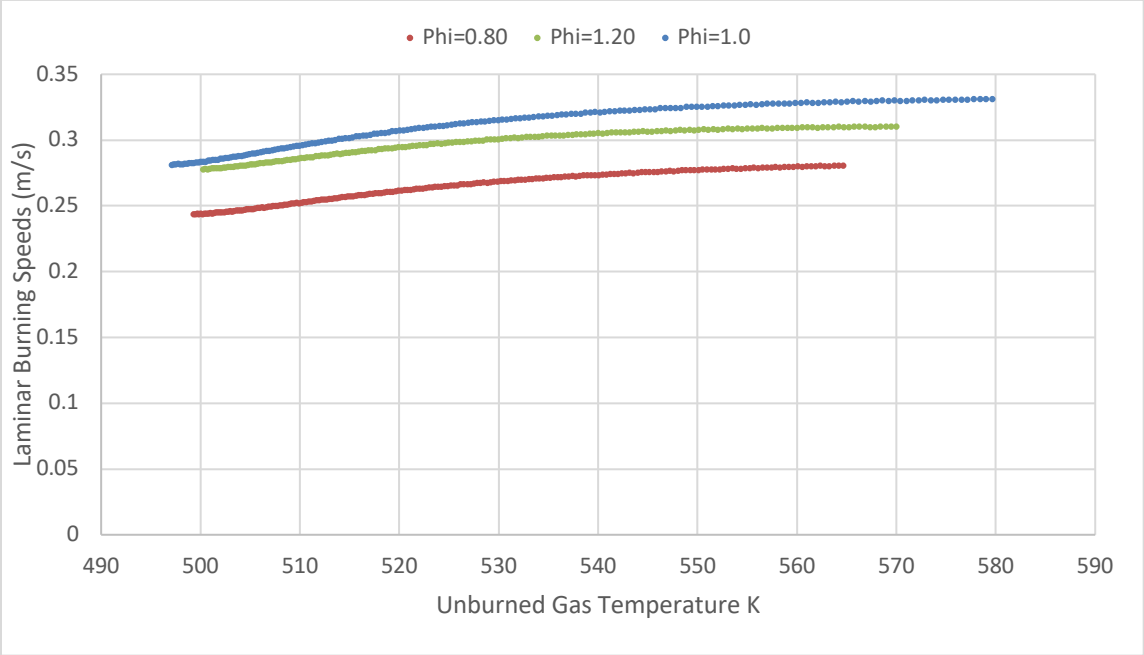

Figure 42: Laminar burning speeds for propane and 80% of carbon dioxide at P_i = 2 atm, T_i = 480 K and different equivalence ratios

Figures 43 shows the conducted experiments at five different concentrations performed at initial temperature of 400 K and atmospheric initial pressure for the fuel-air ratio of 1.1. As shown in Figure 43, the addition of 80% carbon dioxide reduces greatly the laminar burning speeds.

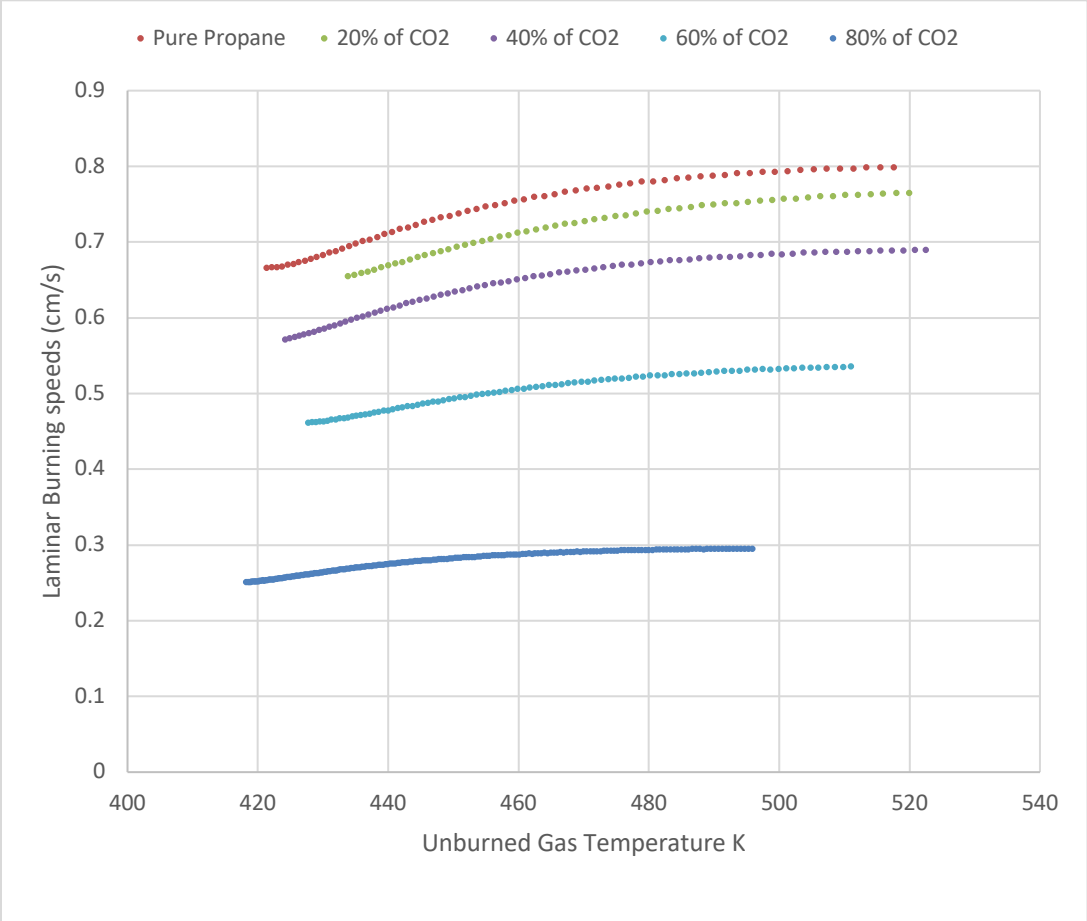

Figure 43: Laminar burning speeds for mixtures of propane with added carbon dioxide concentrations at P_i = 1 atm and equivalence ratio 1.1 at T_i = 400 K

Figures 44 demonstrates the tested experiments at the same different concentrations performed but at elevated initial temperature of 480 K and atmospheric initial pressure for the fuel-air ratio of 1.1.

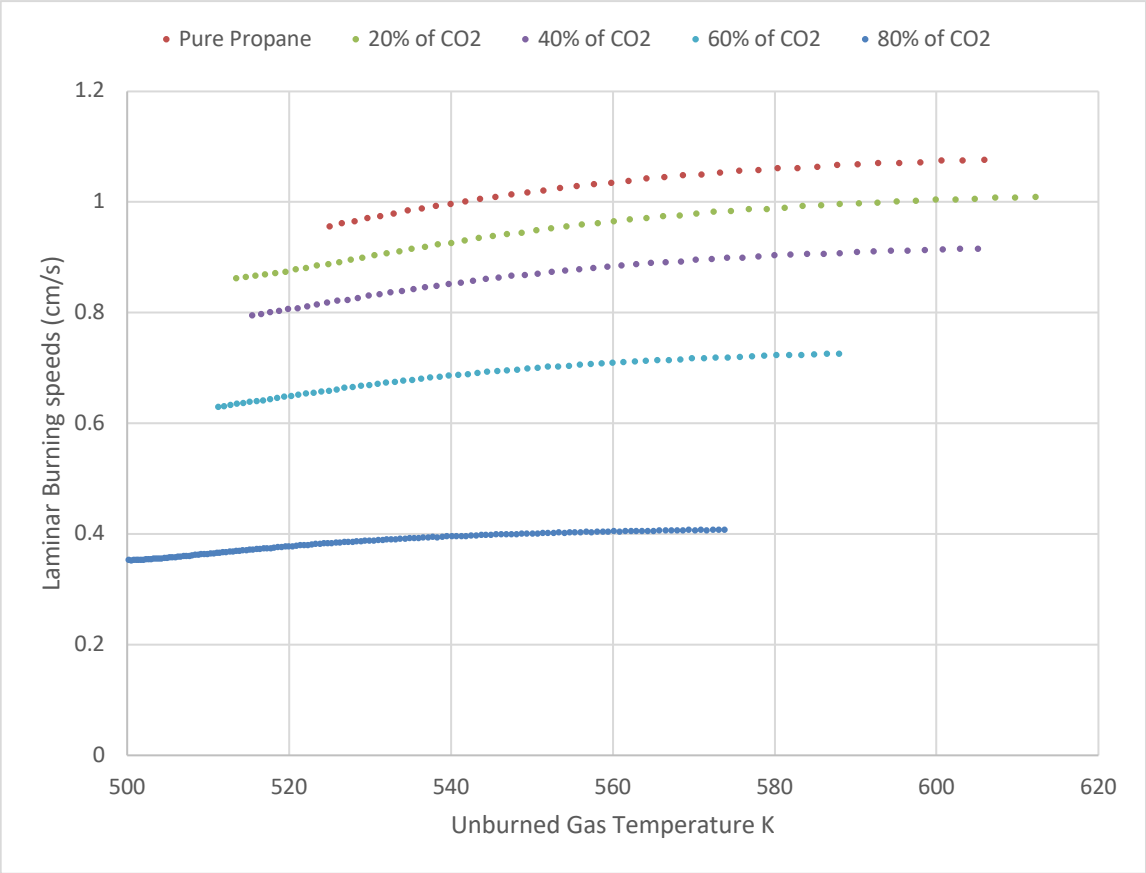

Figure 44: Laminar burning speeds for mixtures of propane with added carbon dioxide concentrations at P_i = 1 atm and equivalence ratio 1.1 at T_i = 480 K

Figure 45 shows data obtained by STANJAN software in three different concentrations to study the reason behind the shift of the fuel-air ratios with the additional of carbon dioxide (CO_2) diluents. The STANJAN software illustrates the peak adiabatic flame temperature as a function of the equivalence ratios. It was observed that as the addition of 80% carbon dioxide, the peak adiabatic flame temperature shifts toward lean mixture. The propane-air (C_3H_8) and 40% of carbon dioxide (CO_2) concentrations, the peak adiabatic flame temperature at Phi=1 and Phi=1.20 is almost own similar peak adiabatic temperatures (2618K and 2620). In contrast, the peak adiabatic flame temperature of Phi=1.0 is higher than the one at Phi=1.20 at both concentrations 60%, and 80%.

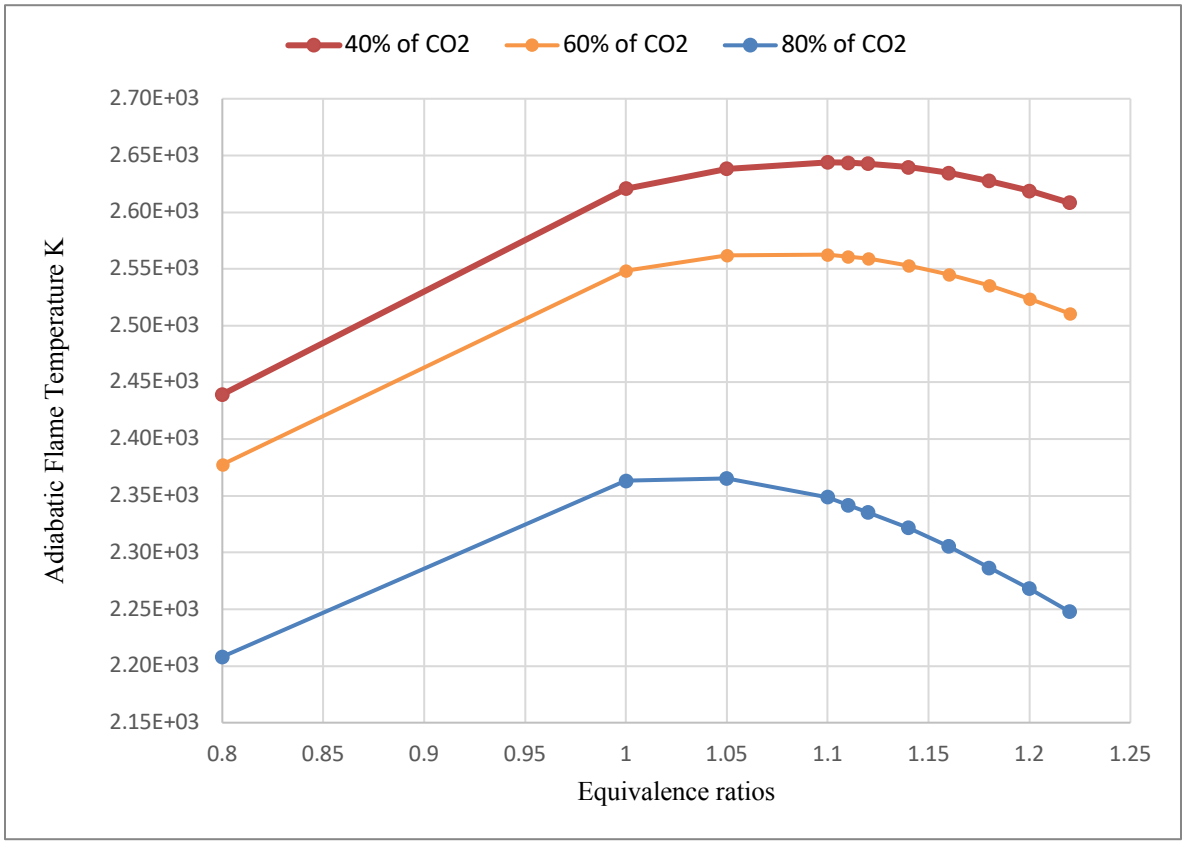

Figure 45: Adiabatic flame temperature data obtained by STANJAN software for 40%, 60%, and 80% of carbon dioxide at P_i = 1 atm, and T_i = 400 K

5. Summary and conclusions

Experimental studies of spherically flame propagation and laminar burning speeds utilizing a thermodynamics model has been conducted using a constant volume cylindrical vessel. The model uses the dynamic pressure rise history as the main input to generate the burning speeds and the flammability characteristic. The shadowgraph setup was employed for the investigation of flame stability and cellularity. To sum up this experimental study, it was revealed that the laminar burning speeds increase as the temperature rises. In contrary, it was noticed that the burning speeds decrease as the pressure increases. Additionally, the result shows that the laminar burning speed decreases as the additional of carbon dioxide concentrations increases since carbon dioxides is classified as non-flammable gaseous fuel. Moreover, the burning speed result shows that the laminar burning speed of pure propane and until 40% of additional carbon dioxide at rich mixtures is higher than the laminar burning speeds of stoichiometric ratio. In contrary, the burning speeds of stoichiometric ratio were higher when the carbon dioxide concentrations exceeded 40 percent. These observations have been seen in the two cases of the initial temperatures of 400 K and 480 K. For rich-mixtures, the collected data is less than the lean mixture as the cellularity development starts earlier and the data have to be restricted to solely smooth flame measurements. Also, both of the stretch effect considerations and the cellularity developments have been well-addressed and taken into accounts in the analysis of determining the burning speed values.

6. References

[1]. Linnett, J. W., Methods of Measuring Burning Velocities, Fourth Symposium (International) on Combustion. 1953. Baltimore: Williams and Wilkins.

[2]. Andrews, G. E. and Bradley D., Determination of Burning Velocities: A Critical Review, Combustion and Flame, 18 (1972), 133-153.

[3]. Rallis C. J. and Garforth A. M., Determination of Laminar Burning Velocity, Progress in Energy and Combustion Science, 6 (1980) 303-329

[4]. J. P. Botha, D. B. Spalding "The laminar flame speed of propane/air mixtures with heat extraction from the flame" Published 6 August 1954. DOI: 10.1098/rspa.1954.0188

[5]. Linteris, G.T. Burning Velocity of 1,1-difluroethane (R-152a), ASHRAE Transactions.

[6]. Wu, C.K., Law, C.K. (1984). On The Determination of Laminar Flame Speeds From Stretched Flames. The Combustion Institute. 1941-1949

[7]. Egolfopoulos, F.N., Cho, P., Law, C.K. (1989). Laminar flame speeds of methane air mixtures under reduced and elevated pressures. Combustion and Flame. 76, 375-391.

[8]. Y.D. Kim M. Matalon "Propagation and extinction of a flame in a stagnation-point flow https://doi.org/10.1016/0010-2180(88)90025-9 Combustion and Flame Volume 73, Issue 3, September 1988, Pages 303-313

[9]. E. Mallard, H.L. Le Chatelier, Ann. Combustion and flame Mines 4 (1883) 379–568

[10]. Eisazadeh-Far, K., Parsinejad, F., Metghalchi, H. (2010). Flame structure and laminar burning speeds of JP-8/air premixed mixtures at high temperatures and pressures. Fuel. 89, 1041- 1049

[11]. Lewis, B., von Elbe, G. (1961). Combustion, Flames, and Explosion of gases, 2nd edition, Academic Press.

[12]. Metghalchi M. and Keck J. C., Burning Velocities of Mixtures of Air with Methanol, Isooctane, and Indolene at High Pressure and Temperature, Combustion and Flame, 48 (1982), 191-210

[13]. Metghalchi, H., Keck, J.C. (1980). Laminar Burning Velocity of Propane-Air Mixtures at High Temperature and Pressure. Combustion and Flame. 38, 143-154.

[14]. Moriya, S.; Yoshida, K.; Shoji, H.; Iijima, A. The effect of uniform and non-uniform electric fields on flame propagation. J. Therm. Sci. Technol. 2008, 3, 254–265.

[15]. Cha, M.S.; Lee, Y. Premixed combustion under electric field in a constant volume chamber.IEEE Trans. Plasma Sci. 2012, 40, 3131–3138.

[16]. Meng, X.W.; Wu, X.M.; Kang, C.; Tang, A.D.; Gao, Z.Q. Effects of direct-current (DC) electric fields on flame propagation and combustion characteristics of premixed CH4/O2/N2 flames. Energy Fuels 2012, 26, 6612–6620.

[17]. . Rahim F., Elia M., Ulinski M., and Metghalchi M., Burning Velocity Measurements of Methane-Oxygen-Argon Mixtures and Its Application to Extend the Methane-Air Burning Velocity Measurements, International Journal of Engine Research, 3 (2) (June 2002), 81-92

[18]. Van Maaren, A, Thung, D.S., De Goey, L.P.H. (1994). Measurement of Flame Temperature and Adiabatic Burning Velocity of Methane/Air Mixtures. Combust. Sci. and Tech. 96, 327-344.

[19]. Takizawa, K., Takahashi, A., Tokuhashi, K., Kondo, S., Sekiya A. (2005). Burning velocity measurement of fluorinated compounds by the spherical-vessel method. Combustion and Flame. 141, 298-307.

[20]. Natarajan, J., Lieuwen, T., and Seitzman, J., 2007, Laminar flame speeds of H2/CO mixtures: Effect of CO2 dilution, preheat temperature, and pressure, Combust. Flame, 151, pp. 104– 119.

[21]. Sanjay Singh, Pushkar Raj, Samir Tamb “Proceedings of the International Conference on Modern Research in Aerospace Engineering: MRAE-2016. pp 11–16